Series analyzed

QC
807.5
.U6
W6 NOAA Technical Memorandum ERL WPL-196
no.196
c.2

IRRADIANCE DISTRIBUTIONS ON THE HUMAN RETINA FROM A LASER OBSERVED THROUGH THE TURBULENT ATMOSPHERE

James H. Churnside
Reginald J. Hill

Wave Propagation Laboratory
Boulder, Colorado
April 1991

noaa NATIONAL OCEANIC AND ATMOSPHERIC ADMINISTRATION / Environmental Research Laboratories

QC
807.5
.U6
W6
no.196
c.2

NOAA Technical Memorandum ERL WPL-196

IRRADIANCE DISTRIBUTIONS ON THE HUMAN RETINA FROM A LASER OBSERVED THROUGH THE TURBULENT ATMOSPHERE

James H. Churnside
Reginald J. Hill

Wave Propagation Laboratory
Boulder, Colorado
April 1991

LIBRARY
JUN 7 - 1991
N.O.A.A.
U.S. Dept. of Commerce

UNITED STATES
DEPARTMENT OF COMMERCE
Robert A. Mosbacher
Secretary

NATIONAL OCEANIC AND
ATMOSPHERIC ADMINISTRATION
John A. Knauss
Under Secretary for Oceans
and Atmosphere/Administrator

Environmental Research
Laboratories
Joseph O. Fletcher
Director

NOTICE

Mention of a commercial company or product does not constitute an endorsement by NOAA/ERL. Use of information from this publication concerning proprietary products or the tests of such products for publicity or advertising purposes is not authorized.

For sale by the National Technical Information Service, 5285 Port Royal Road
Springfield, VA 22161

CONTENTS

Irradiance Distributions on the Human Retina from a Laser Observed through the Turbulent Atmosphere

James H. Churnside
and
Reginald J. Hill

Abstract. The statistics of position and size of the focal spot on a simulated human retina for laser illumination through refractive turbulence in the atmosphere were measured. Both 3-mm and 7-mm apertures were used under a variety of propagation conditions. No significant mitigating effects of spot broadening or motion were observed.

1. INTRODUCTION

In a previous paper (Hill et al., 1987), we measured the statistics of the optical power collected by the human pupil when a laser source is observed through the turbulent atmosphere. We used aperture diameters of 3 mm to simulate the light-adapted pupil and 7 mm to simulate the dark-adapted pupil. We documented instantaneous power levels of more than 80 times the average power level. This implies a significant increase in the ocular hazard of viewing a laser source because of atmospheric turbulence.

That study, which was concerned with total power and the duration of bright events, left unanswered the question of the distribution of the bright spots on the retina. Were high powers associated with a high degree of phase distortion at the pupil? If this were the case, the bright spots might tend to be smeared out, reducing the ocular hazard. They might also tend to come to a focus off the fovea, also reducing the ocular hazard. Here, we answer these questions.

The effect of atmospheric turbulence on imaging systems has long been a topic of interest. Astronomers, in particular, have known that turbulence will smear out the image of a point object. Shapiro (1978) presents a good review of this topic. However, the interest of astronomers and others is generally in the average resolution of an imaging system. The resolution achieved by the instantaneous images that have the highest power has not been investigated.

This paper presents the results of an experimental investigation to determine whether or not phase effects partially

mitigate the amplitude (or scintillation) effects of atmospheric turbulence on ocular safety. Within the limits of sensitivity of our instrumentation, no such mitigating effects exist.

2. DATA ACQUISITION

A series of experiments was performed in the fall of 1989 at the Table Mountain facility north of Boulder, Colorado. A laser transmitter was used to illuminate a receiver under a variety of propagation conditions. The receiver was designed to simulate, as closely as possible, the response of the human eye. Output signals from the receiver were digitized and recorded for processing and statistical evaluation.

The laser was a single-mode, gain-guided GaAlAs diode laser producing 40 mW of radiation at a wavelength near 820 nm. It was mounted on a thermoelectric cooler, and a feedback system was used to maintain the laser heat sink at a constant temperature near 5°C below ambient. In addition, the light out the rear facet of the laser was monitored with photodiode and the laser current was adjusted to maintain a constant value.

The divergence of the beam out of the laser was about 0.5 rad in the vertical direction and about one-half that in the horizontal direction. A 10× microscope objective with a numerical aperture of 0.25 was used to reduce the divergence. At the output of the microscope objective, the power was reduced to about 25 mW and the horizontal beam width was 6 mm. The beam divergence was adjusted depending on path length as follows:

Path length	Horizontal beam divergence
100 m	10 mrad
250 m	5 mrad
500-600 m	2 mrad
>600 m	1 mrad

An electromechanical shutter was placed in front of the microscope objective. This shutter was opened and closed via a radio link from the receiver so background light levels could be periodically measured.

To get a variety of conditions, six paths were used. Four of these were over flat grassland at a nearly uniform height of about 1.5 m. The path lengths of these four were 100 m, 250 m, 500 m, and 1000 m. The next path was a 600-m path across a 40-m-

deep gully. A cross section of the path is presented in Fig. 1, where the solid line represents the terrain level and the dashed line represents the optical beam. The final path was a 9-km path from the foothills of the Rocky Mountains to Table Mountain. This path, shown in cross section in Fig. 2, drops 600 m from the transmitter to the receiver.

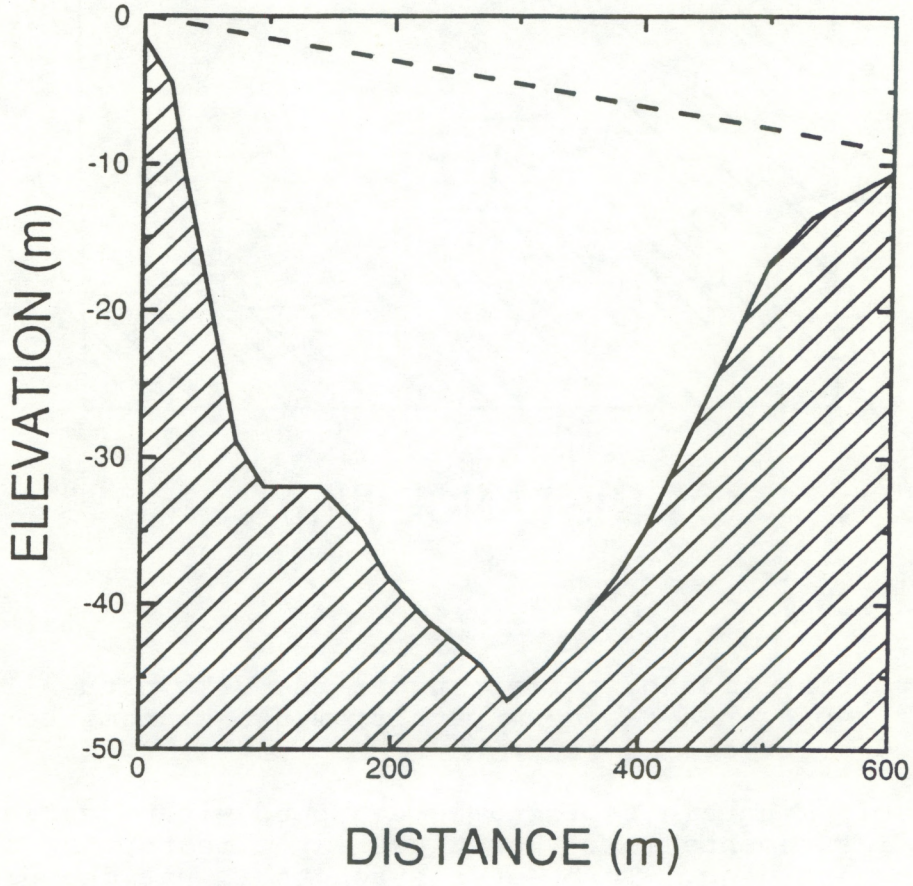

Fig. 1. Cross section of terrain under the 600-m path. The dashed line represents the beam path from the transmitter at (0,0) to the receiver.

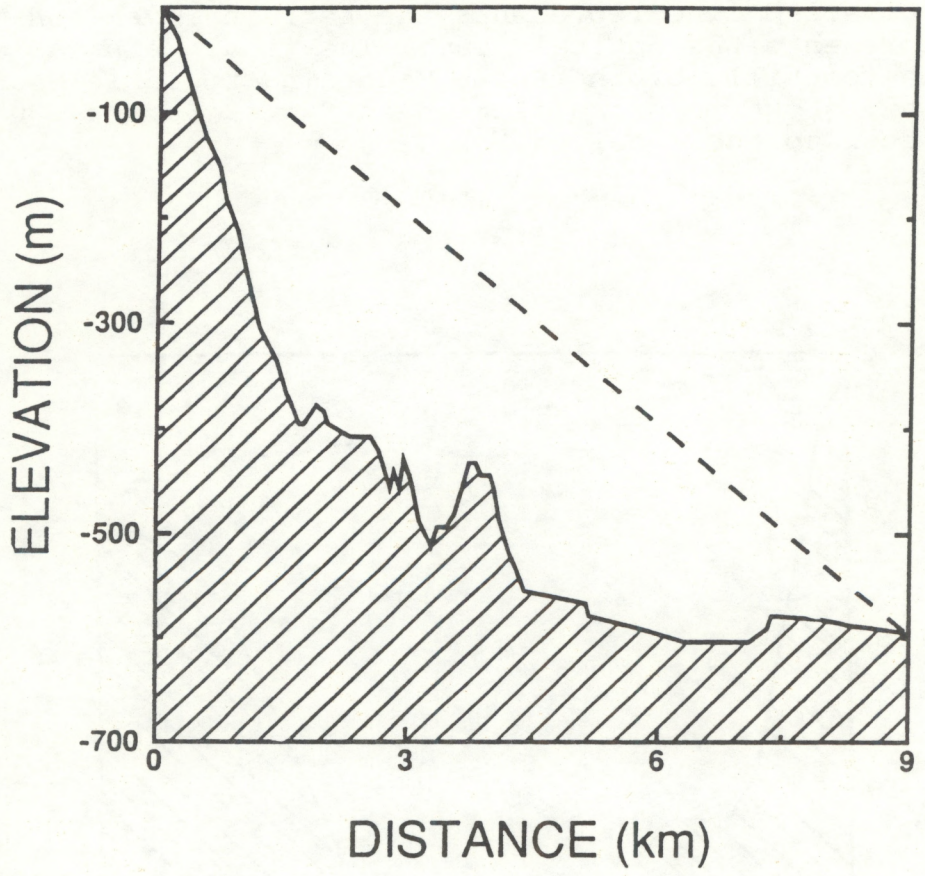

Fig. 2. Cross section of terrain under the 9-km path. The dashed line represents the beam path from the transmitter at (0,0) to the receiver.

The Table Mountain facility is equipped with a variety of turbulence instrumentation. For these experiments, two of these instruments were used. Turbulence strength C_n^2 was measured with a 5-cm-diameter, incoherent scintillometer, described in detail elsewhere (Ochs et al., 1979). It was operating on a 250-m path parallel to the four flat terrain paths and at about the same height. The receiver for this instrument was a few meters away from the experimental receiver. Inner scale, l_o, was measured with a two-channel, coherent/incoherent scintillometer operating on a 150-m path (Ochs and Hill, 1985). This path, at about the same height as the others, was located near the center of the C_n^2 scintillometer path, and crossed it at a small angle (10 mrad). Because of the uniformity of the terrain, these measured values are expected to be representative of the values over the first four paths. They are not useful for the 600-m or 9-km paths, however.

A schematic of the optical receiver is presented in Fig. 3. At the front of the receiver is an aperture. Two different apertures were used; one was 7 mm in diameter to simulate the dark-adapted pupil, and the other was 3 mm to simulate the light-adapted pupil. Behind the aperture, a narrow band interference filter blocked background light while allowing the laser light to pass through. This filter had a 70-nm pass band centered at 810 nm.

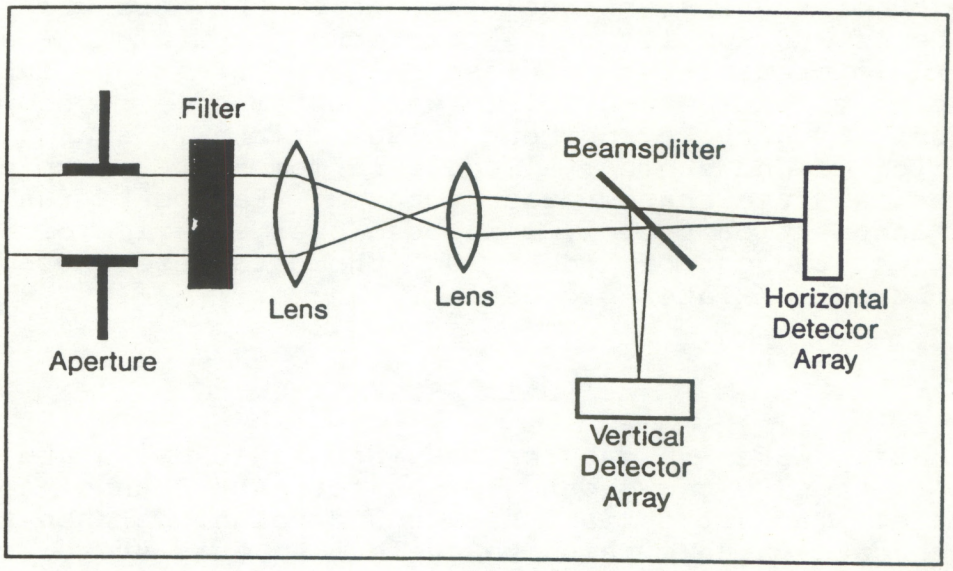

Fig. 3. Opto-electronic receiver used to simulate the human eye.

A two-element compound lens behind the filter focused the light onto the detector arrays. The first lens had a focal length of 25 cm. The second lens had a focal length of 1 cm. The separation of the two lenses was adjusted to slightly more than 26 cm to produce a focused spot on the detector arrays for collimated light. The effective focal length of this two-lens system was measured by rotating the receiver through a known angle and observing the displacement of the spots on the detectors; the value was 3.1 m.

A beamsplitter divided the energy between the horizontal and vertical detector arrays. Each array comprised 20 silicon detector elements, each 0.28 mm by 6.45 mm. The center-to-center spacing of the elements was 0.31 mm, so the total area of the array was 6.48 mm by 6.45 mm. The only difference between the

two arrays was their orientation. Each detector element was fed into a transimpedence preamplifier with a gain of 10^5 V/A and a bandwidth greater than 10 kHz. Each of the 40 preamp outputs was equipped with a sample-and-hold circuit, and the resulting signals were multiplexed into a single analog-to-digital converter in a PC-type microcomputer.

The data acquisition software began by triggering the 40 sample-and-hold circuits. It then stepped the multiplexer through all 40 channels, digitizing each one with a 12-bit analog-to-digital converter and storing the result in memory. After 3750 of these 40-channel samples of the data were collected at a rate of 200 samples per second, the computer sent a signal to the radio transmitter to close the shutter at the laser, and 300 samples of background levels were obtained. To complete the data acquisition cycle, current values of the C_n^2 and I_o signals were digitized and stored, all data in memory were copied to the hard disk, and the shutter was reopened. Each data run comprised 30 such acquisition cycles, collected over a period of about 30 minutes. At the end of a data run, the data were stored on magnetic tape for later processing.

3. DATA PROCESSING

The first step in data processing was to calculate the average of the 300 background levels for each channel for each data cycle. The appropriate background value was then subtracted from each data value within the cycle. At this stage, we noticed an additional offset of about -15 to -25 mV (out of a digitizer range of 10 V) when the shutter was open and the array was illuminated. This offset was estimated by assuming that the average illumination on the outermost three elements on each side of each array was small. The offsets for these six elements on each array were averaged and used to correct each element in that array.

A typical plot of the voltage across one of the arrays after background and offset correction is presented as a solid line in Fig. 4. This particular example was taken from the horizontal array behind the 7-mm-diameter aperture, with illumination over the 100-m path.

To get an estimate of the total power incident on the aperture for each sample, we summed the voltages of the individual elements across each array. That is, the signal power voltage S_V was found from

$$S_V = \sum_{i=1}^{20} V_i, \tag{1}$$

where V_i was the voltage on the i'th element of the array under consideration.

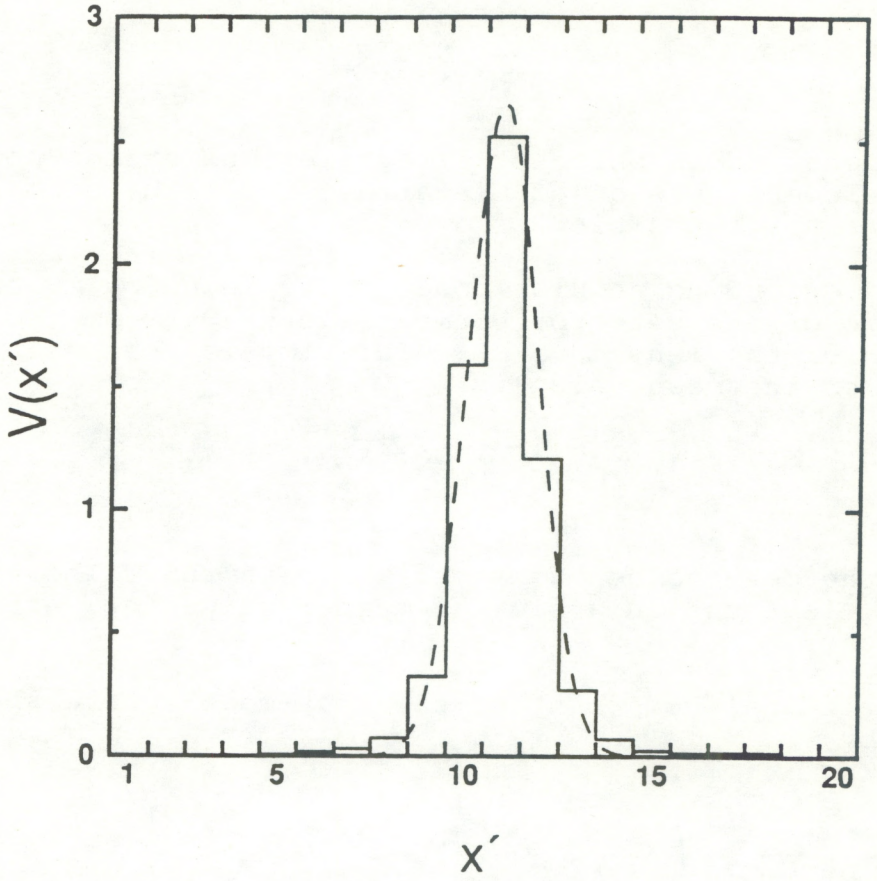

Fig. 4. Example of the voltage V as a function of position x' across one of the 20-element arrays. The solid line represents the voltage across each element and the dashed line represents a fit to the Gaussian shape.

The horizontal component of the position of the centroid of the spot in the focal plane is defined by

$$x = \frac{\int_{-\infty}^{\infty} dx' \int_{-\infty}^{\infty} dy'\, x'\, I(x', y')}{\int_{-\infty}^{\infty} dx' \int_{-\infty}^{\infty} dy'\, I(x', y')}, \qquad (2)$$

where x' and y' are the horizontal and vertical position in the focal plane, and I is the irradiance in the focal plane. Since

each detector element integrates the irradiance over y' and over a small region of x', we can get an estimate of the horizontal position from the voltages produced by the horizontal array as follows:

$$x = \frac{1}{S_V} \sum_{i=1}^{20} i\, V_i, \tag{3}$$

where x is measured in units of array elements from a point one-half of an element outside of the array (i.e., the center of the first element has a position of $x' = 1$).

The corresponding angular position is found by multiplying x by the ratio of the detector element width (0.31 mm) to the focal length of the lens (3.1 m). This implies that the angular deviation from the mean value is

$$\alpha_x = 10^{-4}(x - \bar{x}), \tag{4}$$

where $\bar{x}$ is the mean value of x over the data run. The vertical component α_y is found in a similar manner using the vertical array voltages.

The horizontal component of the root-mean-square spot width is defined by

$$w_x/2 = \left[\frac{\int_{-\infty}^{\infty} dx' \int_{-\infty}^{\infty} dy'\, x'^2\, I(x', y')}{\int_{-\infty}^{\infty} dx' \int_{-\infty}^{\infty} dy'\, I(x', y')} - x^2 \right]^{1/2}. \tag{5}$$

The obvious technique to obtain an estimate of this quantity from the array voltages is to let

$$w_x = 2 \left[\frac{1}{S} \sum_{i=1}^{20} i^2\, V_i - x^2 \right]^{1/2}. \tag{6}$$

However, this approach was very sensitive to noise during deep, turbulence-induced fades (i.e., when S_V was small).

A less noise-sensitive technique was desired. The solution was to assume that the focal plane spot was nearly Gaussian with a total area of S_V, a mean position of x, and a width w_x. The

voltage that this spot would produce from each element in the array was calculated and these voltages were compared to the measured values. The width w_x was adjusted to minimize the sum of the squares of these differences.

The formula for the assumed Gaussian voltage distribution in one dimension is

$$V(x') = \frac{S_V}{w_x}\sqrt{\frac{2}{\pi}}\exp\left[-\frac{2}{w^2}(x' - x)^2\right]. \tag{7}$$

This is plotted as a dashed line in Fig. 4. For this case, S_V = 6.20 V, x = 9.95 elements, and w_x = 1.85 elements. If we estimate w_x using Eq. (6), we obtain a value of 2.18 elements, which is 18% higher. The difference, however, is due to the edges of the spot, which are not important to eye-safety issues. If we recalculate w_x using Eq. (6) but using only the main part of the peak (detector elements 8-12), we obtain a value of 1.86. Therefore, the Gaussian fit was considered a better method for obtaining w_x than Eq. (6).

The horizontal component of angular width is given by

$$\omega_x = 10^{-4}\, w_x, \tag{8}$$

where 10^{-4} represents the same ratio of element size to focal length. The vertical width w_y and its corresponding angular width ω_y are found in the same manner using the vertical array voltages.

These algorithms were used to calculate estimates of power, position, and width for each array for each sample of data. These processed data were stored for statistical analysis. The pertinent statistics for each data run are summarized in Appendix A.

4. RESULTS

The first data run after testing, designated 20, was obtained using a path length of L = 100 m and an aperture diameter of D = 7 mm. The measured turbulence level was C_n^2 = 8.9 ± 1.9 × 10^{-13} $m^{-2/3}$, where the ± value represents the atmospheric variability in the 30 samples and not measurement errors. Similarly, the measured inner scale was 5.7 ± 0.6 mm.

For spherical wave propagation through weak turbulence, the variance of the normalized irradiance can approximated by (Lawrence and Strohbehn, 1970)

$$\sigma_I^2 = 0.5k^{7/6}L^{11/6}C_n^2 \quad \text{for } l_o << (\lambda L)^{1/2} \tag{9a}$$

$$= 1.28L^3 l_o^{-7/3} C_n^2 \quad \text{for } l_o >> (\lambda L)^{1/2}, \tag{9b}$$

where λ is the optical wavelength, $k = 2\pi/\lambda$ is the optical wave number, and the Tatarskii spectrum (Lawrence and Strohbehn, 1970) was assumed in Eq. (9b). We also use the weak turbulence variance given by the right-hand side of Eq. (9a) to define the scintillation index β. For the 100-m path of this case, the Fresnel zone size $(\lambda L)^{1/2}$ was 9.1 mm. Since $l_o < (\lambda L)^{1/2}$, we use Eq. (9a) to estimate σ_I^2 even though the condition $l_o << (\lambda L)^{1/2}$ is not satisfied. The result is $\sigma_I^2 = 0.22$.

The variance of the normalized power through an aperture of diameter D can be approximated by (Churnside, 1991)

$$\sigma_S^2 = \left[1 + 0.362(D^2/\lambda L)^{7/6}\right]^{-1} \sigma_I^2. \tag{10}$$

The calculated value was $\sigma_S^2 = 0.18$. The measured values from the horizontal array $\sigma_{S_x}^2$ and from the vertical array $\sigma_{S_y}^2$ were both 0.17, which is very close to the predicted value. We should point out that a more exact expression for σ_s^2 exists (Lawrence and Strohbehn, 1970). It is based on the correct spectrum of turbulence (Hill and Clifford, 1978) and requires numerical integration using tabulated spectral values. Since we are not interested in a detailed comparison of theory and experiment for σ_s^2, the simpler approximation described above was used. In addition, the correlation between the power measured by the two arrays was 0.9995. Since both arrays used the same aperture, unity correlation was expected, and a value this close implies that the noise from the detectors is low.

We expect the probability density function of normalized signal power, $S = S_v/\langle S_v \rangle$, to have a lognormal form for a 3- or 7-mm aperture under a wide variety of turbulence conditions (Hill et al., 1987; Churnside and Hill, 1987; Churnside and Clifford, 1987). A histogram of the probability density function of power as measured by the vertical array is presented in Fig. 5. The dashed line is a lognormal density function with the same variance, and we see that the measured density function is indeed lognormal.

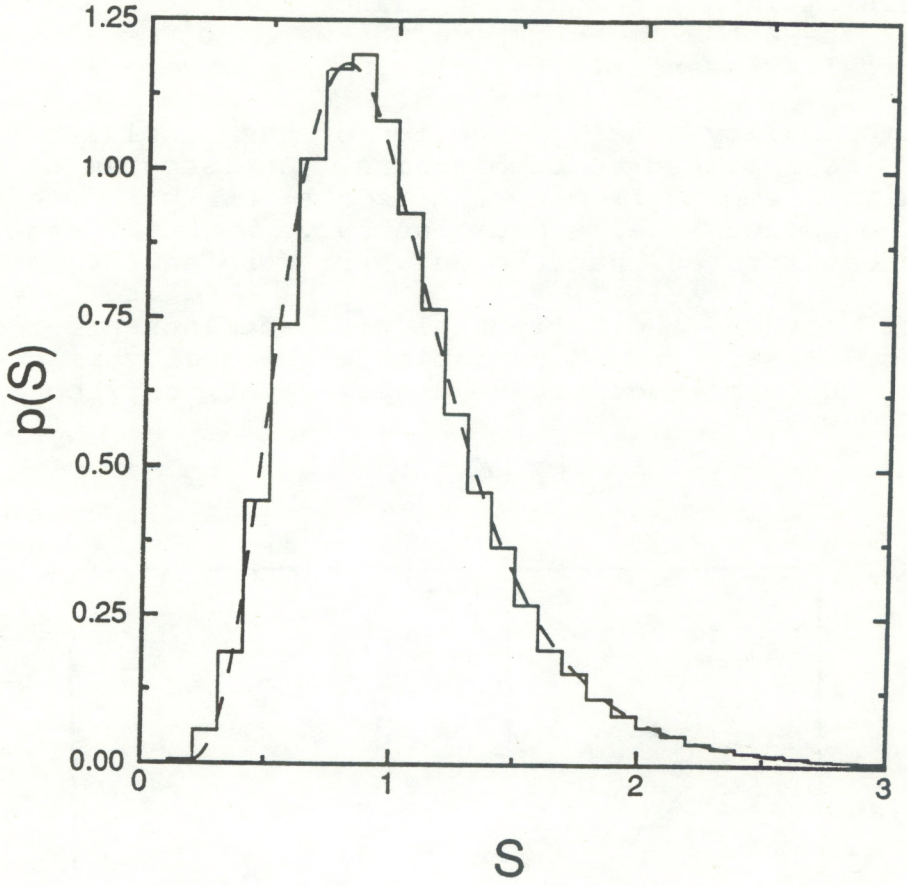

Fig. 5. Probability density function p(S) of normalized signal power S from vertical array with 7-mm aperture and 100-m path. Solid line is measured histogram and dashed line is a lognormal density function with variance of 0.17.

The variance of the angle-of-arrival fluctuations in each axis is approximately (Lawrence and Strohbehn, 1970; Churnside and Lataitis, 1987)

$$\sigma_\alpha^2 = 2k^{-2}\rho_o^{-5/3}D^{-1/3}, \tag{11}$$

where the phase coherence length is

$$\rho_o = (0.54k^2LC_n^2)^{-3/5} \quad \text{for} \quad l_o << \rho_o \tag{12a}$$

$$= (0.62k^2Ll_o^{-1/3}C_n^2)^{-1/2} \quad \text{for} \quad l_o >> \rho_o. \tag{12b}$$

The calculated coherence length for run 20 was 8.5 mm using Eq. (12a). This implies an angular variance of $\sigma_{\alpha}^2 = 5.0 \times 10^{-10}$ for each axis. The actual measured values were $\sigma_{\alpha_x}^2 = 7.5 \times 10^{-10}$ for the horizontal axis and $\sigma_{\alpha_y}^2 = 8.4 \times 10^{-10}$ for the vertical axis.

The probability density function of the displacement in a single axis is expected to be Gaussian. A histogram of the measured displacements from the horizontal array is plotted in Fig. 6. The dashed line, a Gaussian curve with the same variance, demonstrates that the data are very nearly Gaussian.

If the vertical and horizontal displacements are zero-mean, independent Gaussian random variables with equal variance, we expect that the magnitude of the displacement, defined as

$$|\alpha| = \left(\alpha_x^2 + \alpha_y^2\right)^{1/2}, \tag{13}$$

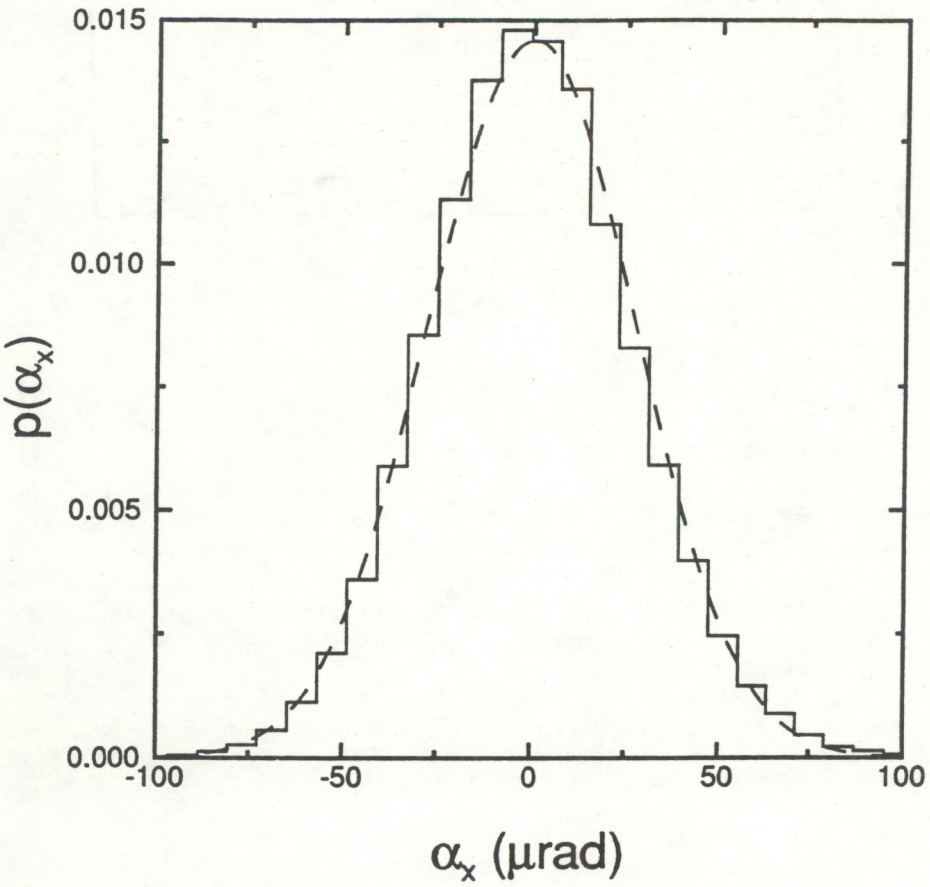

Fig. 6. Probability density function $p(\alpha_x)$ of horizontal angular displacement α_x using 7-mm aperture and 100-m path. Solid line is measured histogram and dashed line is a Gaussian density function with variance of 7.5×10^{-10}.

would be a Rayleigh random variable. If we use the average value of $\sigma_\alpha^2 = 7.9 \times 10^{-10}$ for both axes, we find that the magnitude should have a mean value of $|\overline{\alpha}| = 35$ μrad and a variance $\sigma^2_{|\alpha|} = 3.4 \times 10^{-10}$. The actual measured values were 35 μrad and 3.6×10^{-10}, respectively. A histogram of the measured displacement magnitude is plotted in Fig. 7, along with a Rayleigh density function with $|\overline{\alpha}| = 35$ μrad. We see that the distribution is nearly Rayleigh, as expected.

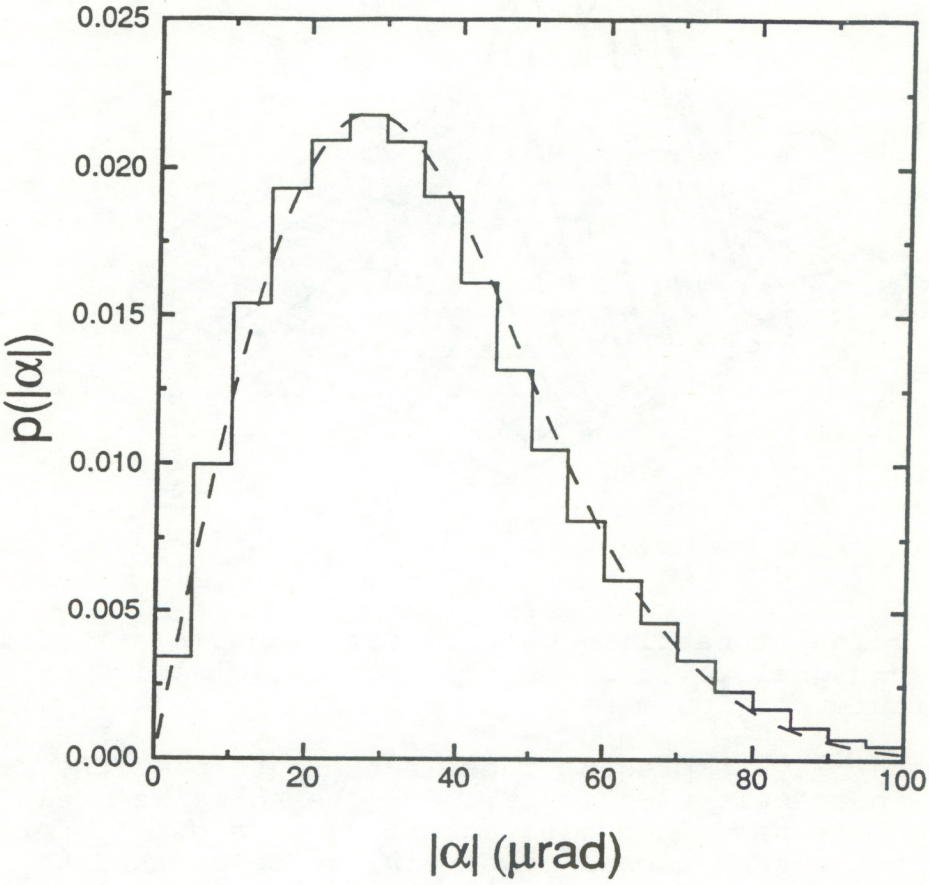

Fig. 7. Probability density function $p(|\alpha|)$ of magnitude of angular displacement $|\alpha|$ using 7-mm aperture and 100-m path. Solid line is measured histogram and dashed line is Rayleigh density function with mean of 35 μrad.

The joint probability density function of the vertical displacement and the signal power is plotted in Fig. 8. We see no large trend in either the peak or the width of the density function along the displacement axis as the signal level changes. The correlation coefficient between displacement and power for this case was -0.03, which supports this conclusion.

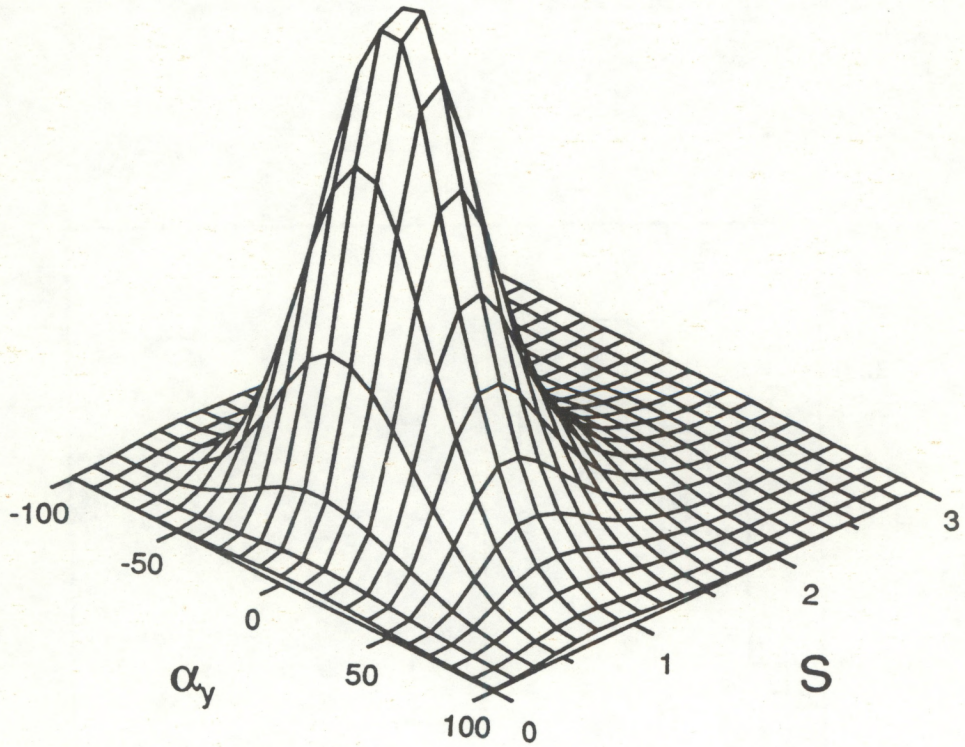

Fig. 8. Joint probability density function $p(S, \alpha_y)$ of the normalized signal power S and the vertical displacement α_y using 7-mm aperture and 100-m path.

Another way to present these data is to plot the magnitude of the displacement as a function of the normalized signal power. We grouped the data into bins according to signal power. For the data points in each signal power bin, we calculated the mean and standard deviation of the magnitude of the deviation. The results are presented in Fig. 9; the sides of each box represent the boundaries of the signal power bin, and the top and bottom represent the mean deviation plus and minus the standard deviation, respectively. Again, we see no significant trends in either the mean displacement or the fluctuations of displacement with increasing signal power.

If the spot in the focal plane were diffraction limited, the spot shape would be the well-known Airy function. Unfortunately, the root-mean-square width of the Airy function is undefined (the

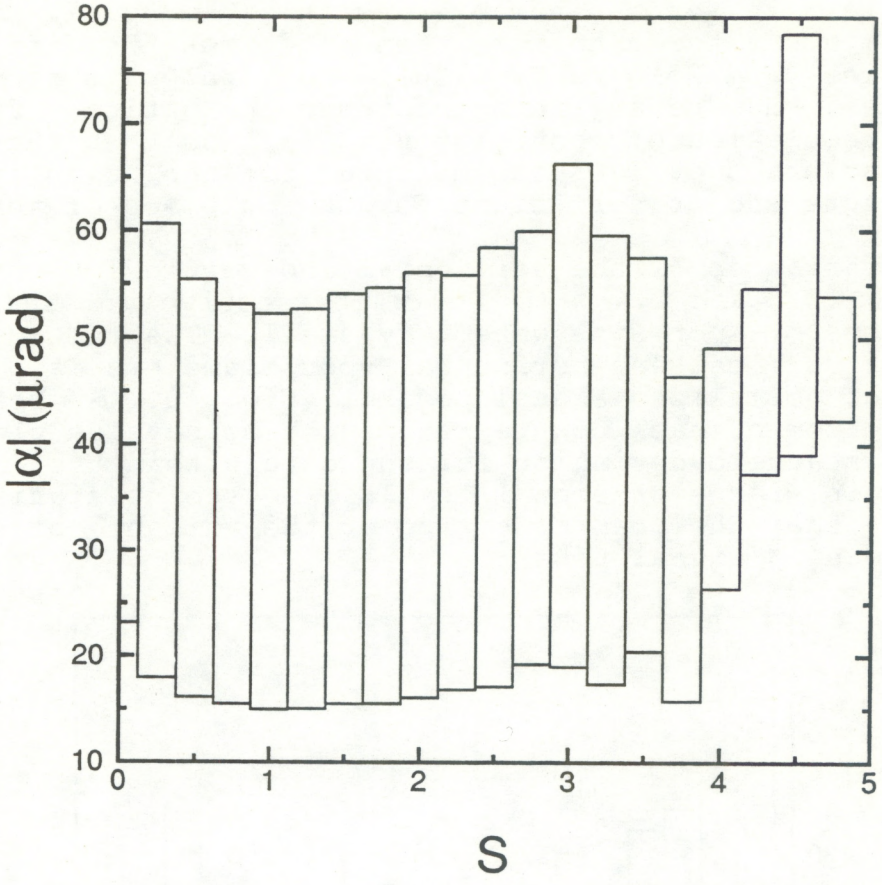

Fig. 9. Magnitude of angular displacement $|\alpha|$ as a function of normalized signal power S. Top and bottom of each box represent mean of $|\alpha|$ plus and minus one standard deviation for the data in the corresponding range of S values.

integral does not converge). Hence, to compare our results to the diffraction limit, we observe that the Airy function has a full width at one-half maximum that is the same as a Gaussian function with a root-mean-square width of

$$\omega_D = 5.5/kD. \tag{14}$$

For the 7-mm aperture, ω_D = 100 μrad.

The mean measured spot size in both directions was 180 μrad. Since the phase coherence length ρ_o was slightly larger than the aperture diameter, we expect that the average spot diameter would be near the diffraction limit. A bench measurement of the spot size produced by the receiver also yielded a value of 180 μrad. We conclude that our optics are not diffraction limited for a 7-mm diameter and that aberrations, probably dominated by spherical aberration, limit the spot diameter to about 180 μrad.

For comparison, we note that measurements of the minimum blur circle size for the human eye with a 7-mm pupil diameter range from about three to more than six times the diffraction limit (Sliney and Wolbarsht, 1980). As with our system, the difference is due to aberrations within the optics. Thus, our "visual" resolution of about 180 μrad is less than the minimum visual resolution of 300 μrad measured for the human eye with a 7-mm aperture and is sufficient for the purposes of this study.

The variances of the horizontal and vertical spot diameters were 1.6×10^{-10} and 1.4×10^{-10} rad^2, respectively. The fluctuations of spot size were very small. The root-mean-square average of vertical and horizontal spot diameters is plotted as a function of normalized signal power in Fig. 10. As before, the top and bottom of each box represent the mean value plus and minus one standard deviation for the data within the corresponding range of signal levels. We see no significant trend of either the mean spot size or the variance of spot size with increasing signal power.

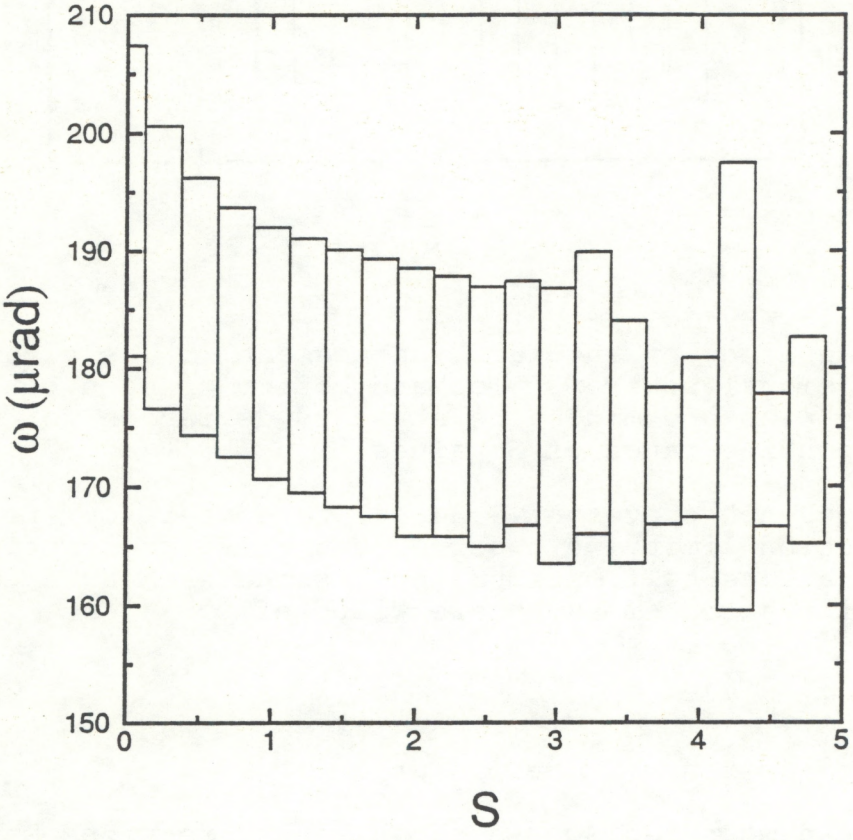

Fig. 10. Root-mean-square average of the horizontal and vertical spot diameters ω as a function of normalized signal power *S*. Top and bottom of each box represent mean of ω plus and minus one standard deviation for the data in the corresponding range of *S* values.

The next case, run 21, was obtained over the same path but with a 3-mm-diameter aperture. The turbulence level was slightly higher, at $C_n^2 = 9.4 \pm 1.9 \times 10^{-13}$ $m^{-2/3}$, and the inner scale was also slightly larger, at $l_o = 5.9 \pm 0.7$ mm. The calculated scintillation index was also higher for this case, at $\beta = 0.23$. The larger 3-mm aperture provides only a small degree of aperture averaging, so the calculated signal variance was 0.22.

Measured values of 0.29 on both the horizontal and vertical arrays are close to this calculated value. The measured correlation between the two channels was 0.994. The smaller aperture collects less power, and the signal-to-noise ratio is therefore lower. This results in a lower correlation coefficient than that observed for the 7-mm aperture. The probability density function of the vertical array and the corresponding lognormal density function are presented in Fig. 11. As before, the signal power is nearly lognormal.

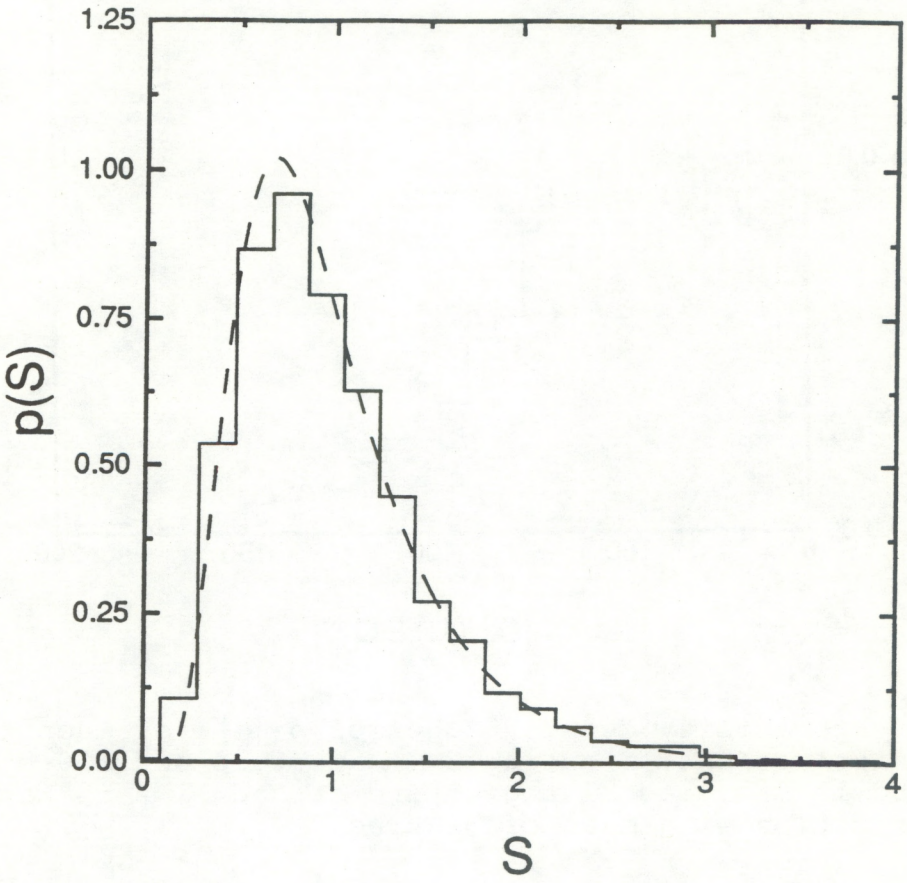

Fig. 11. Probability density function p(S) of normalized signal power S from vertical array with 3-mm aperture and 100-m path. Solid line is measured histogram and dashed line is a lognormal density function with variance of 0.29.

The predicted angular variance for each axis was 7.1×10^{-10}. The measured values were 2.4×10^{-9} for the horizontal axis and 2.1×10^{-9} for the vertical axis. The mean value of the magnitude of the angular deviation was 54 μrad and the variance was 1.5×10^{-9}. Figure 12 is a histogram of the displacement magnitudes and a Rayleigh density function with a mean value of 54 μrad. The distribution is still nearly Rayleigh, although the agreement is not as good as in the previous case. It is distorted by a number of large displacement values that are not consistent with the Rayleigh model.

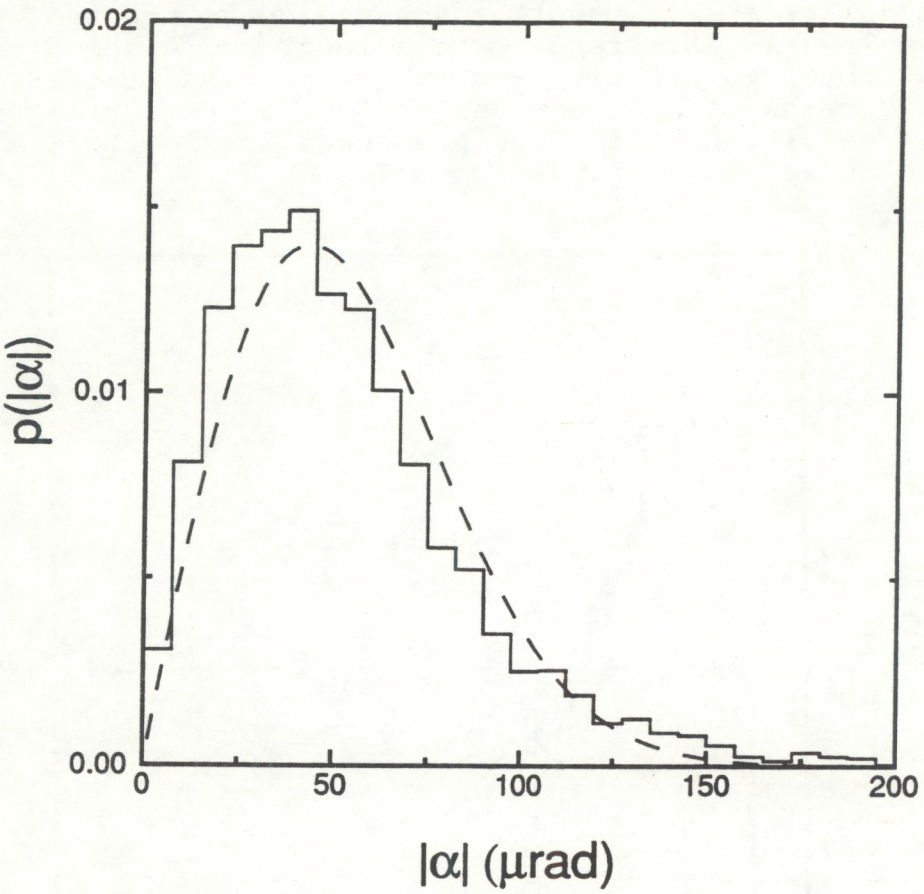

Fig. 12. Probability density function $p(|\alpha|)$ of magnitude of angular displacement $|\alpha|$ using 3-mm aperture and 100-m path. Solid line is measured histogram and dashed line is Rayleigh density function with mean of 54 μrad.

Figure 13 is a plot of the joint probability density function of the vertical displacement and the signal power. Note that at very low signal levels, the distribution of angles is large. In the limit of zero power, the spot position is undefined; at low signal levels, it is very sensitive to noise

from the detectors. Thus, large values can result during signal fades. This explains the deviation from Rayleigh statistics and also the -0.37 correlation between signal power and the magnitude of the displacement.

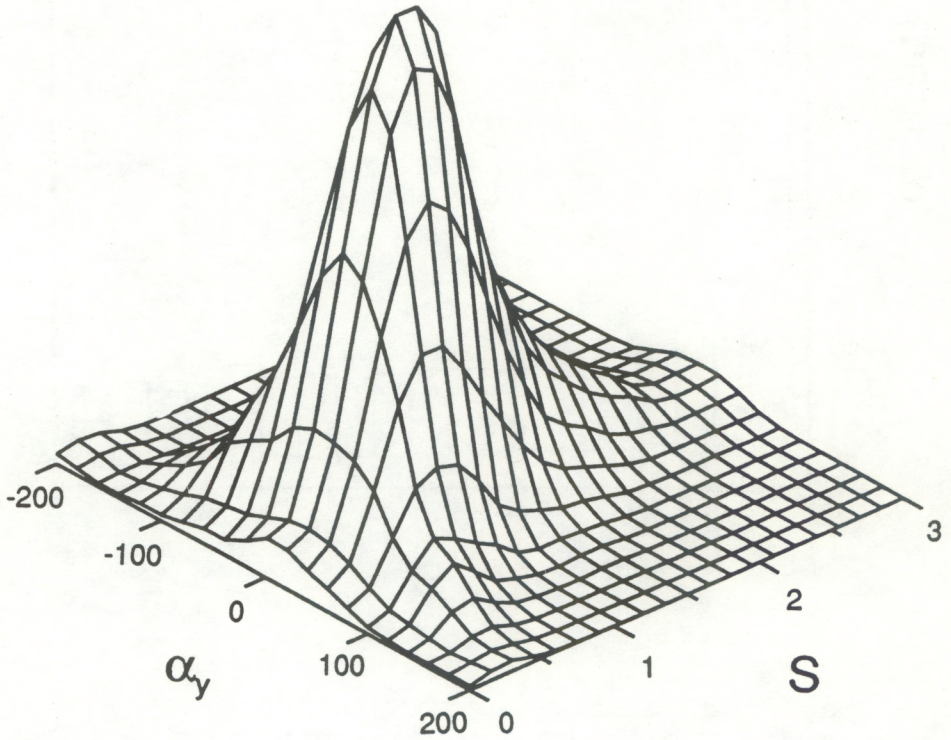

Fig. 13. Joint probability density function $p(S, \alpha_y)$ of the signal power S and the vertical displacement α_y using 3-mm aperture and 100-m path.

Figure 14 is a plot of the magnitude of the displacement as a function of signal level. Here, the large displacement and large fluctuations of the displacement at very low signal levels are very evident. However, for signal levels greater than about half of the mean, no significant trend in either the mean level or the fluctuations can be seen.

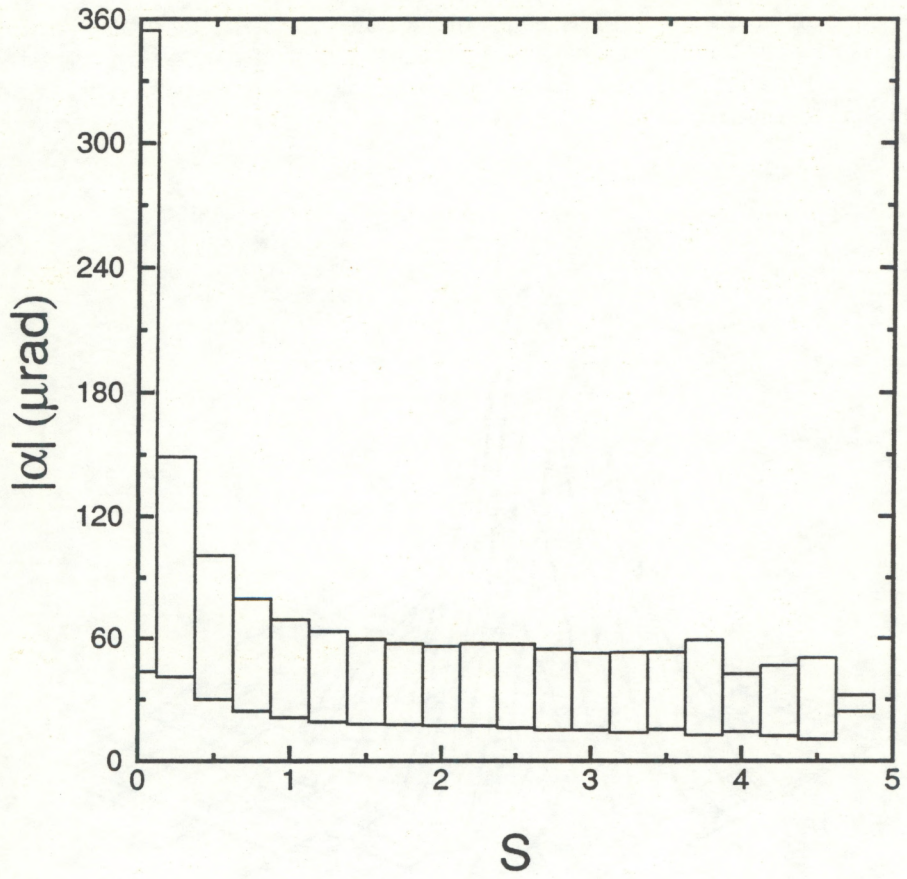

Fig. 14. Magnitude of angular displacement $|\alpha|$ as a function of normalized signal power S. Top and bottom of each box represent mean of $|\alpha|$ plus and minus one standard deviation for the data in the corresponding range of S values.

For the 3-mm-diameter aperture, the diffraction limited spot diameter is ω_D = 240 μrad. A bench measurement yielded a value of 230 μrad. The average value of the measured diameter was 230 μrad along the horizontal axis and 240 μrad along the vertical axis; we conclude that the 3-mm aperture was diffraction limited for this run. The measured values for the variance of spot diameter were $\sigma^2_{\omega_x} = 2.5 \times 10^{-10}$ and $\sigma_{\omega_y} = 3.3 \times 10^{-10}$. Thus the fluctuations of spot diameter are much smaller than the diffraction limit, and it appears that the atmosphere has no significant effect on the retinal image under the conditions of this run.

The spot diameter is plotted as a function of signal power in Fig. 15. We see that the estimated values are lower at small signal levels and also have larger fluctuations in this region. For signal levels greater than the mean, however, there appears

to be no significant dependence of either the average spot diameter or of the fluctuations of spot diameter on signal power.

Runs 36 and 37 were also obtained over a 100-m path with aperture diameters of 7 mm and 3 mm, respectively. The statistics for these runs are summarized in Appendix A. The results are similar to runs 20 and 21 and are not discussed here.

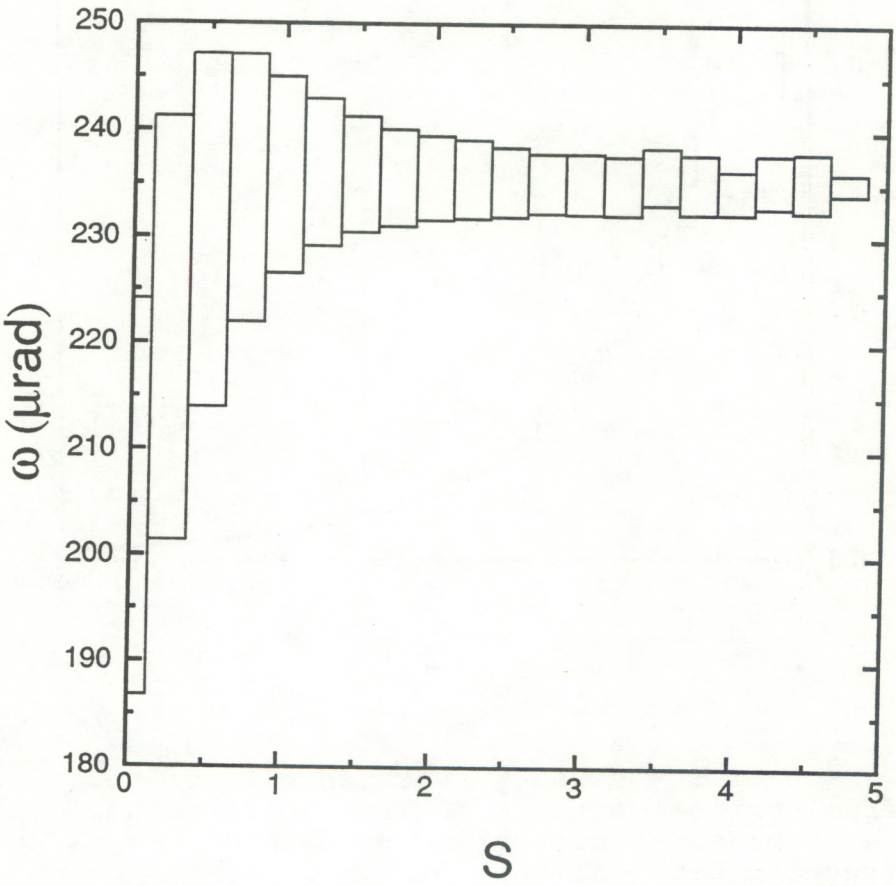

Fig. 15. Root-mean-square average of the horizontal and vertical spot diameters ω as a function of normalized signal power S. Top and bottom of each box represent mean of ω plus and minus one standard deviation for the data in the corresponding range of S values.

The next two cases were obtained over a 250-m path. For run 22, a 7-mm-diameter aperture was used. The turbulence parameters for this run were $C_n^2 = 8.5 \pm 2.4 \times 10^{-13}$ $m^{-2/3}$ and $l_o = 5.5 \pm 0.5$ mm. The calculated scintillation index was 1.1 and, because of the 1.4-cm Fresnel zone, we expect the signal variance to be about this same value. The measured signal variance of each array was 1.3. The correlation between the signals from the two channels was 0.9996. The probability density function of power is approximately lognormal, as Fig. 16 shows.

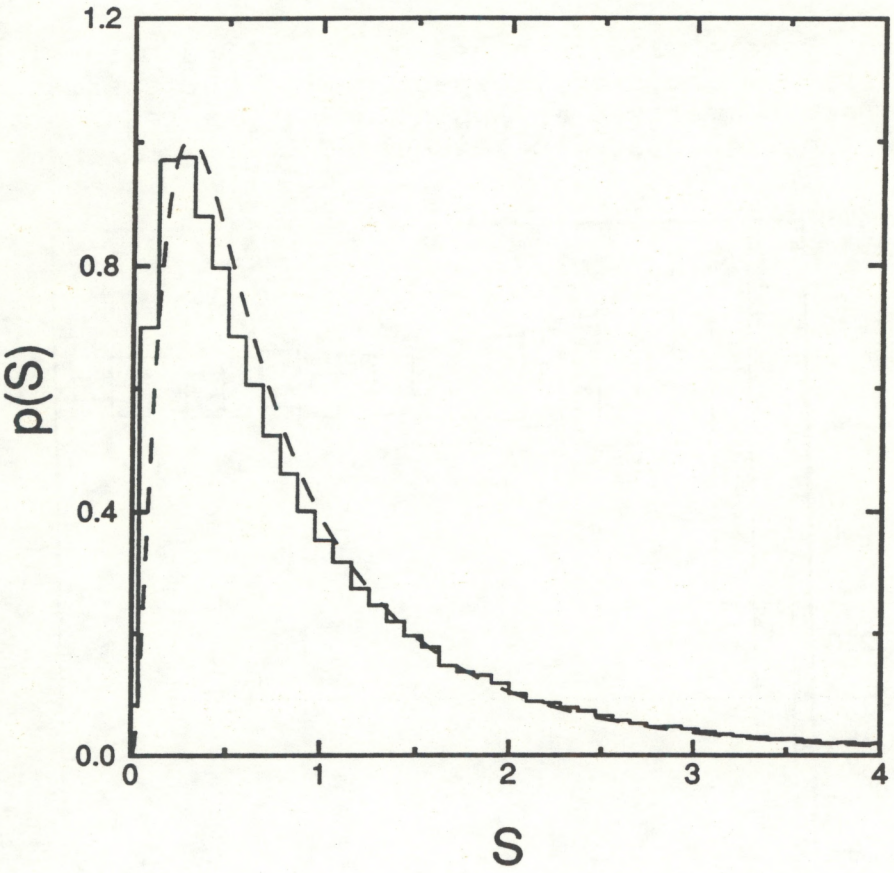

Fig. 16. Probability density function p(S) of normalized signal power S from vertical array with 7-mm aperture and 250-m path. Solid line is measured histogram and dashed line is a lognormal density function with variance of 1.3.

From (11), the predicted angular displacement variance is 1.1×10^{-9}. Measured values were 3.7×10^{-9} for the horizontal axis and 4.5×10^{-9} for the vertical axis. The mean value of the magnitude of the angular deviation was 67 μrad and the variance was 3.4×10^{-9}. Figure 17 shows that the magnitude of the displacement is approximately Rayleigh, although the agreement is not as good as in run 20. In run 22, the signal variance is higher. This results in more deep fades, which produce erroneous estimates of the displacement. As in run 21, deep fades produce higher probabilities at large displacements and distort the density function.

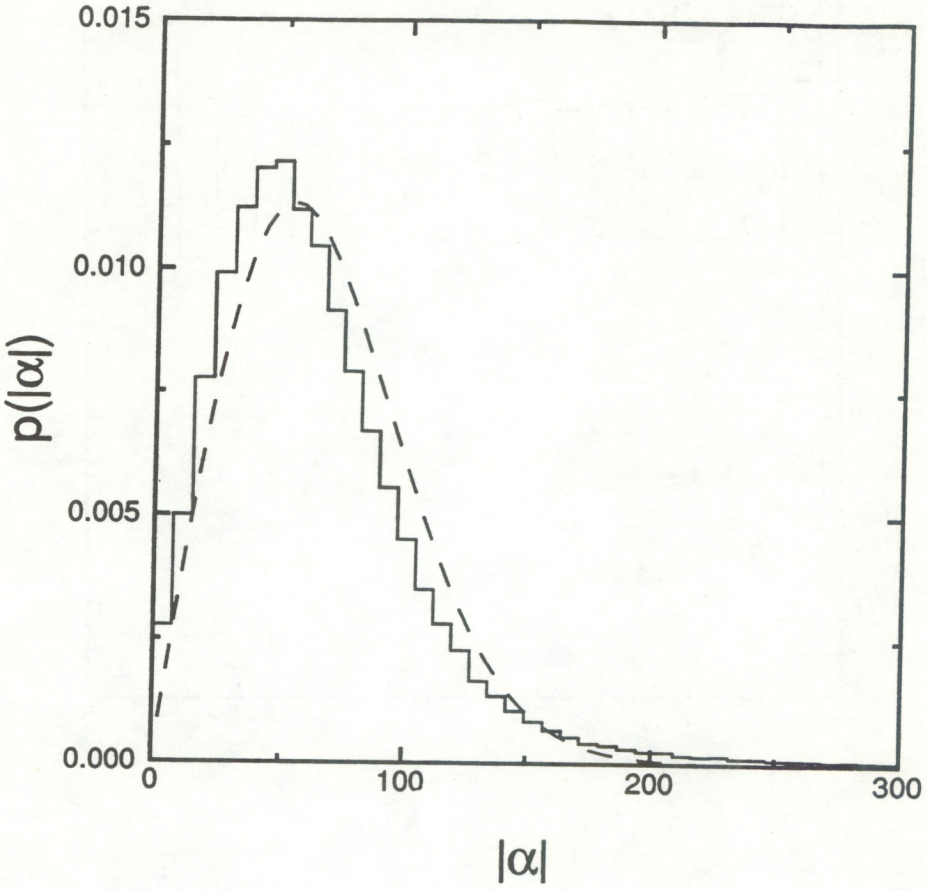

Fig. 17. Probability density function $p(|\alpha|)$ of magnitude of angular displacement $|\alpha|$ using 7-mm aperture 250-m path. Solid line is measured histogram and dashed line is Rayleigh density function with mean 67 μrad.

The magnitude of the displacement is plotted as a function of normalized signal power in Fig. 18. The bin at zero signal is very large because of noise; it had to be compressed by a factor of 50 to fit on the same scale as the rest of the bins. Beyond that, no significant dependence of either the mean value or the level of fluctuations on signal power is seen.

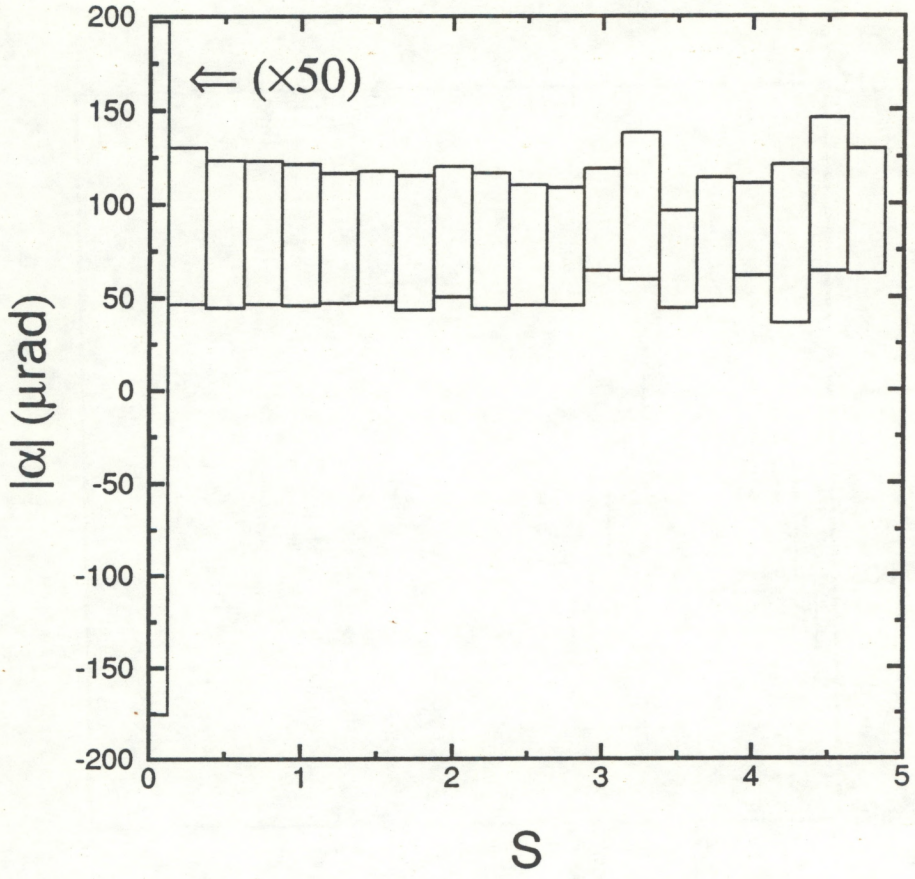

Fig. 18. Magnitude of angular displacement $|\alpha|$ as a function of normalized signal power S. Top and bottom of each box represent mean of $|\alpha|$ plus and minus one standard deviation for the data in the corresponding range of S values.

As in run 20, the mean spot angular diameter in each axis was 170 μrad, the resolution limit. The variances were 7.2×10^{-10} in the horizontal and 7.7×10^{-10} in the vertical. The spot size is plotted as a function of signal power in Fig. 19. No dependence on signal levels is observed.

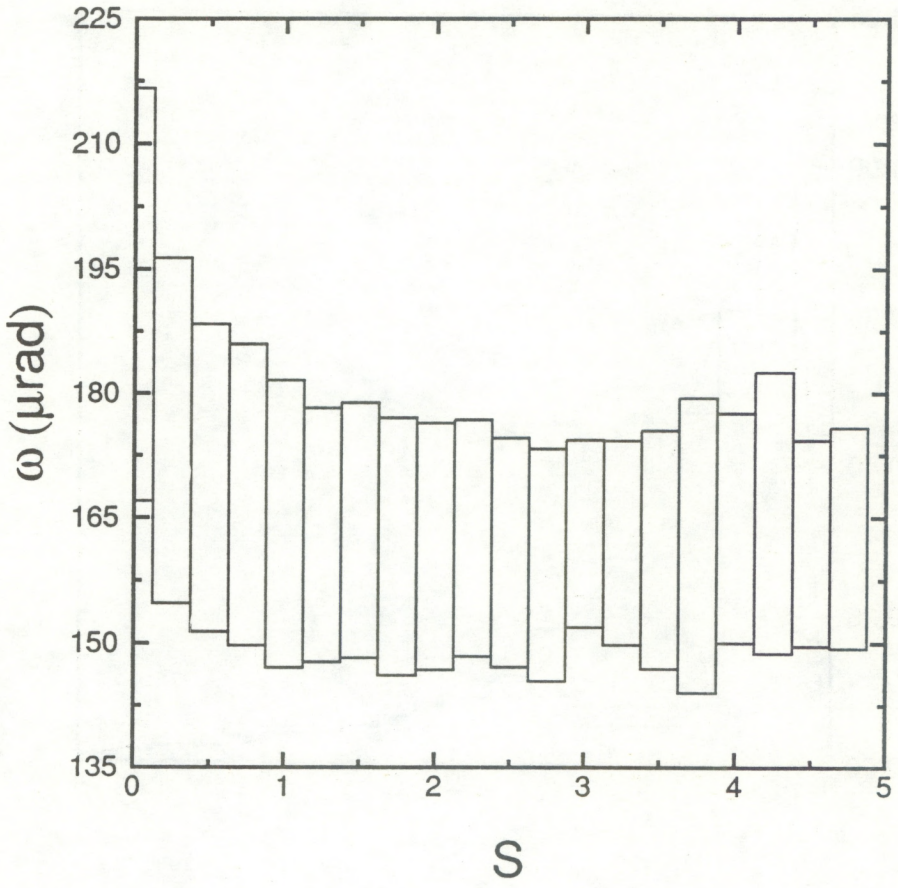

Fig. 19. Root-mean-square average of the horizontal and vertical spot diameters ω as a function of normalized signal power S. Top and bottom of each box represent mean of ω plus and minus one standard deviation for the data in the corresponding range of S values.

In run 23, a 3-mm-diameter aperture was used. The turbulence parameters during this run were $C_n^2 = 8.3 \pm 1.8 \times 10^{-13}$ $m^{-2/3}$ and $l_o = 5.7 \pm 0.7$ mm. The calculated scintillation index was $\beta = 1.1$, which agreed well with the measured variance of 1.2 on each array. The correlation of the power on the two arrays was 0.9995. The probability density function, presented in Fig. 20, is nearly log normal.

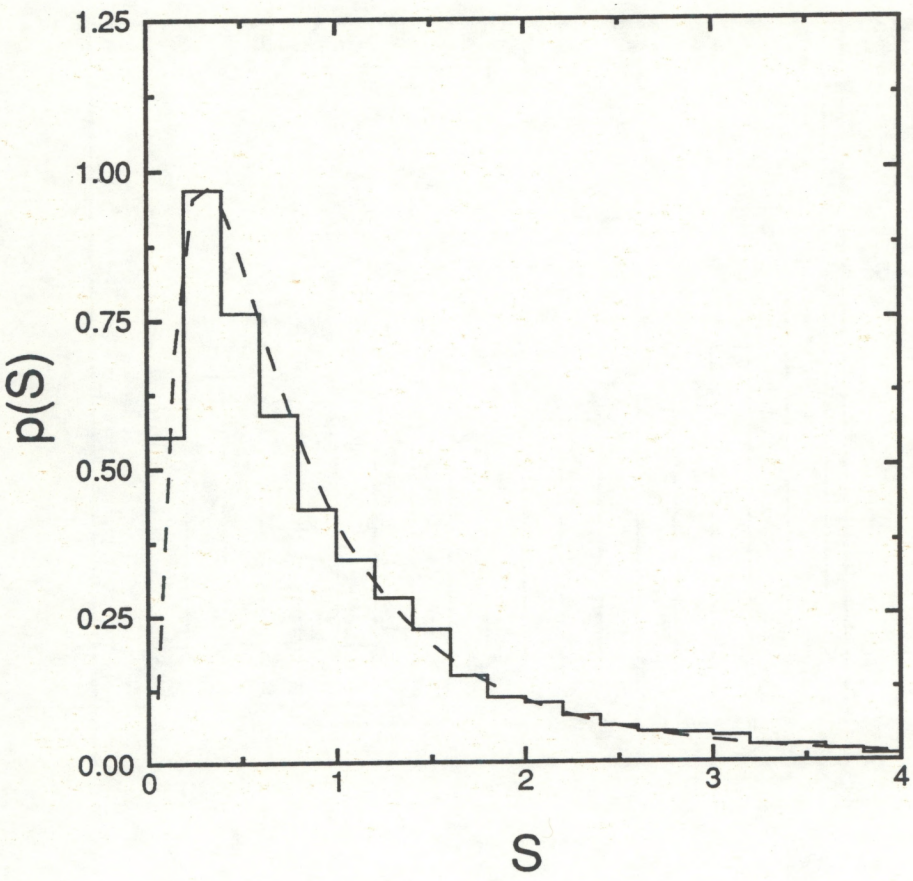

Fig. 20. Probability density function p(S) of normalized signal power *S* from vertical array with 3-mm aperture and 250-m path. Solid line is measured histogram and dashed line is a lognormal density function with variance of 1.2.

The predicted variance of angular displacement for this case is 1.5×10^{-9}. The measured values were much higher: 2.4×10^{-8} in the horizontal axis and 2.9×10^{-8} in the vertical axis. The mean of the magnitude of the displacement was 130 μrad. The probability density function of displacement magnitude is plotted in Fig. 21. It shows a substantial deviation from Rayleigh because of a substantial number of very large displacements. The reason for this is clear from the plot of the displacement magnitude as a function of signal power in Fig. 22. The 3-mm aperture collects less optical power than the 7-mm aperture does. This means that the signal-to-noise ratio is lower and the displacement estimate is too large when the signal level is below its mean value. At signals above the mean, no dependence on signal level is observed.

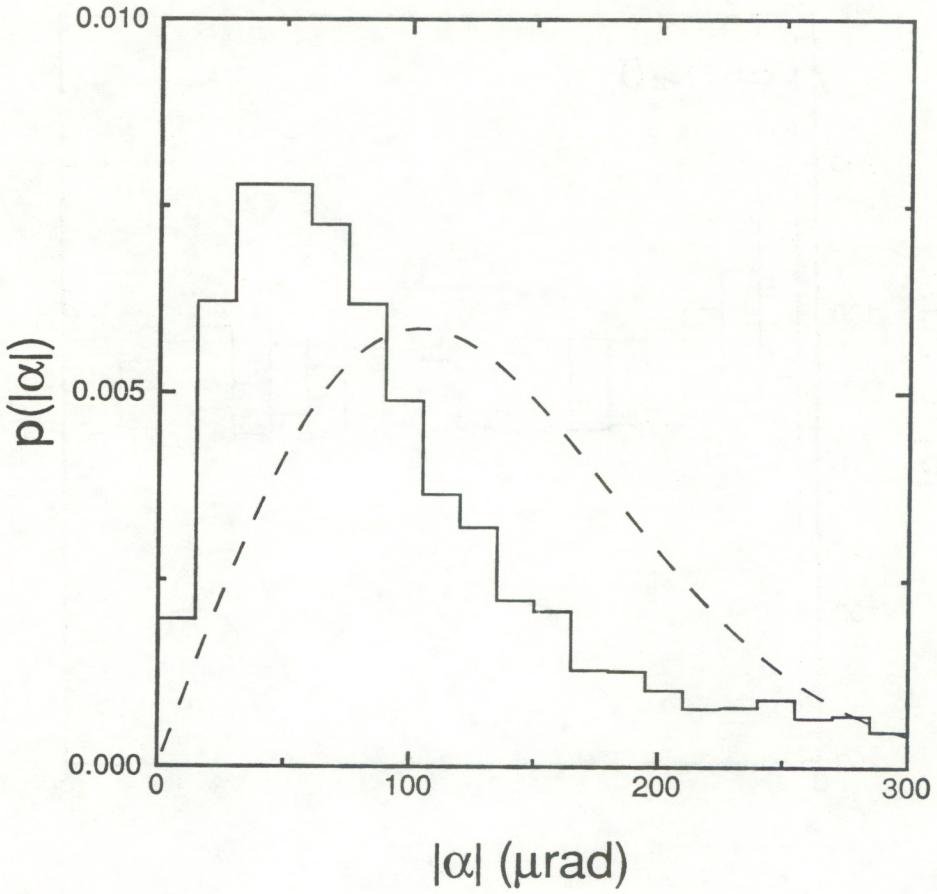

Fig. 21. Probability density function p(|α|) of horizontal angular displacement |α| using 3-mm aperture and 250-m path. Solid line is measured histogram and dashed line is a Rayleigh density function with of 130 μrad.

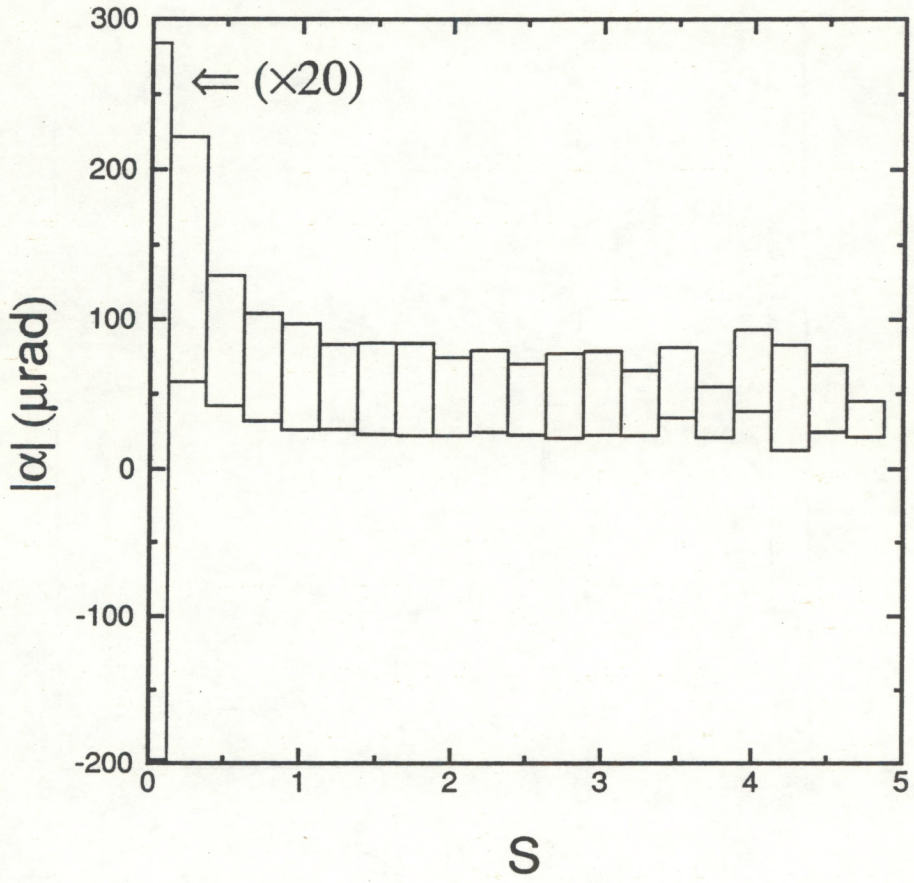

Fig. 22. Magnitude of angular displacement $|\alpha|$ as a function of normalized signal power S. Top and bottom of each box represent mean of $|\alpha|$ plus and minus one standard deviation for the data in the corresponding range of S values.

The mean value of the measured spot diameter for this run was 220 μrad in the horizontal axis and 230 μrad in the vertical. We conclude that we are diffraction limited for this run. The plot of spot diameter as a function of signal level, shown in Fig. 23, shows that the fluctuations of spot diameter are small and that the fluctuations and the mean value are independent of signal level for signal levels above the mean. At very low signal levels, the estimates of spot diameter are affected by noise.

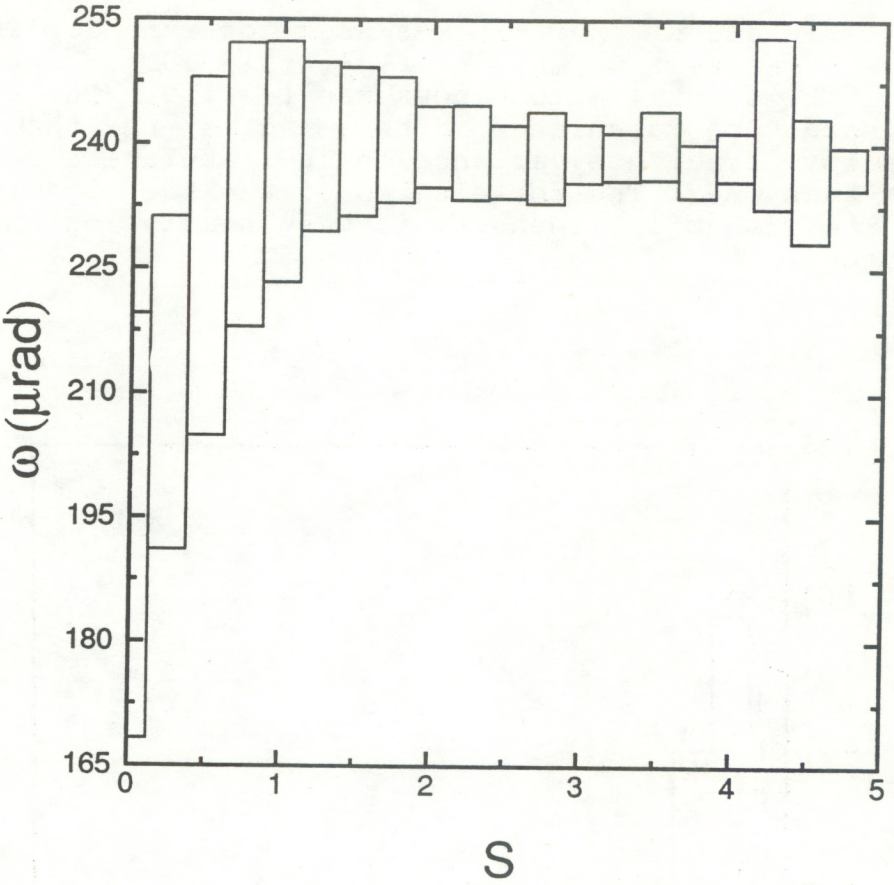

Fig. 23. Root-mean-square average of the horizontal and vertical spot diameters ω as a function of normalized signal power *S*. Top and bottom of each box represent mean of ω plus and minus one standard deviation for the data in the corresponding range of *S* values.

Runs 34 and 35 were also obtained over a 250-m path. The statistics are summarized in Appendix A, although some of the theoretical values could not be calculated because of a failure of the inner-scale instrument during these runs. The results of runs 34 and 35 are similar to those of 22 and 23, and they are not discussed here.

Runs 24 and 25 were obtained over a 500-m path. However, no data were obtained from run 25 because of a misaligned

receiver. The available statistics are presented in Appendix A for completeness, but they are not discussed. Instead, we present runs 32 and 33, which were taken on the same path.

A 7-mm-diameter aperture was used for run 33. The turbulence parameters were $C_n^2 = 4.1 \pm 1.0 \times 10^{-13}$ $m^{-2/3}$ and $l_o = 7.0 \pm 0.6$ mm. The scintillation index was $\beta = 1.9$. The signal power variance cannot be calculated in this regime; the theory is not available for irradiance variance in the saturation regime where β is larger than one. The correlation of the two signals was 0.9995. The probability density is very nearly log normal, as Fig. 24 shows.

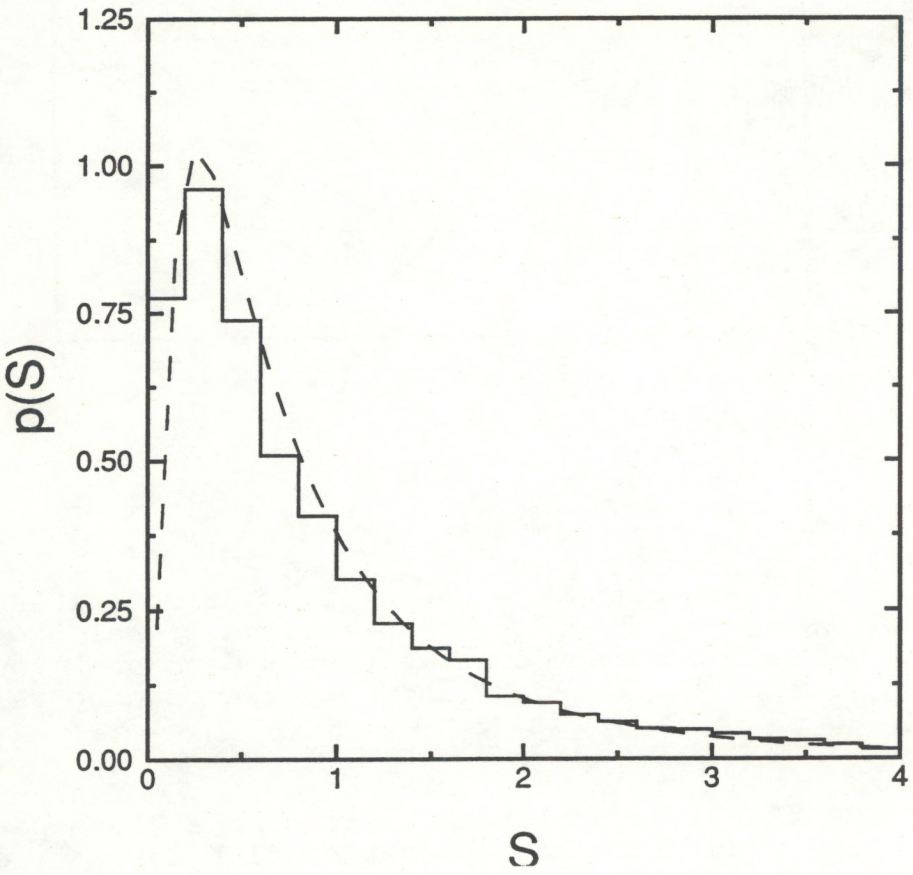

Fig. 24. Probability density function p(S) of normalized signal power S from vertical array with 7-mm aperture and 500-m path. Solid line is measured histogram and dashed line is a lognormal density function with variance of 1.4.

The predicted displacement variance for this case was 1.1 × 10^{-9}. The measured values were higher at 5.5 × 10^{-9} for the horizontal axis and 8.8 × 10^{-9} for the vertical axis. The measured mean of the magnitude of the displacement was 73 μrad. In this case as well, deep signal fades result in large estimates of displacement, and the probability density function of displacement is not Rayleigh. This is clearly shown in Fig. 25. Figure 26, a plot of displacement magnitude as a function of signal power, shows larger displacements at low signal levels. No trend is evident for signals above about one-half of the mean value.

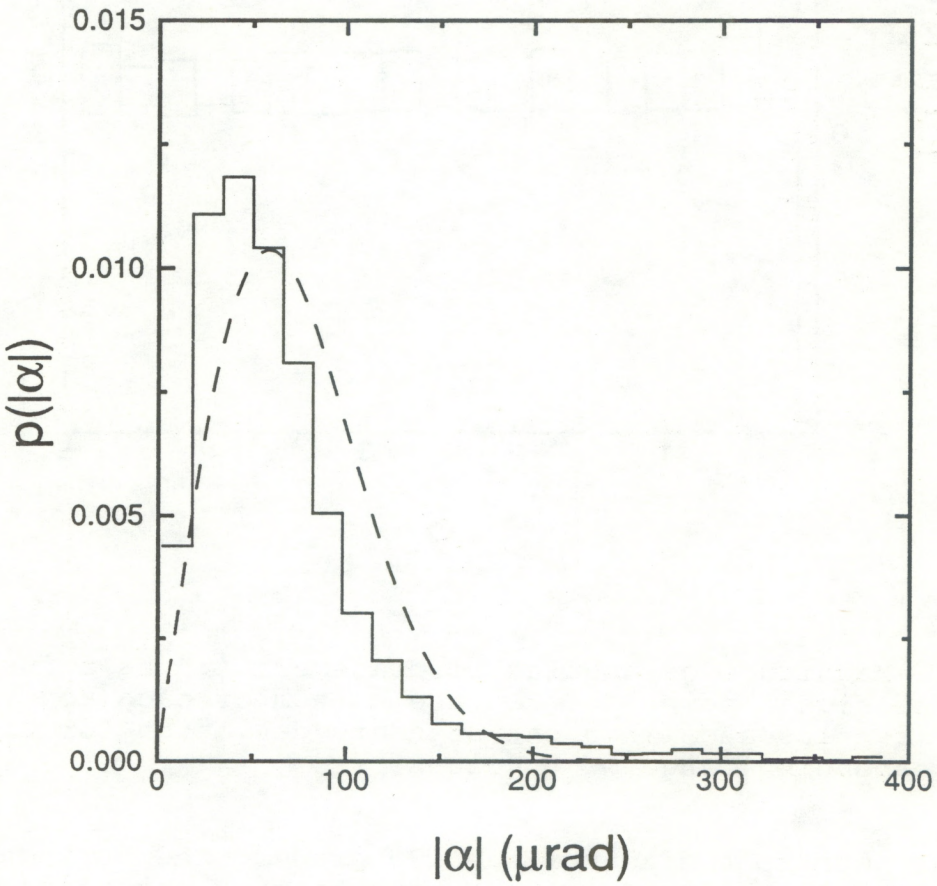

Fig. 25. Probability density function p(|α|) of horizontal angular displacement |α| using 7-mm aperture and 500-m path. Solid line is measured histogram and dashed line is a Rayleigh density function with of 73 μrad.

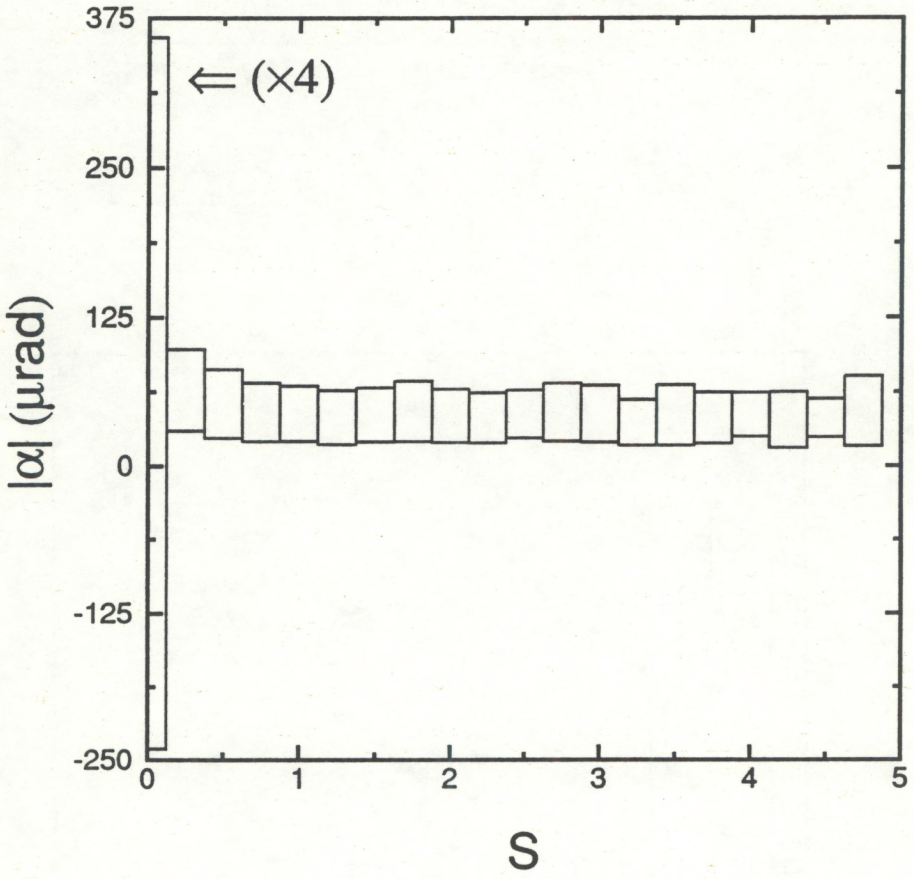

Fig. 26. Magnitude of angular displacement $|\alpha|$ as a function of normalized signal power S. Top and bottom of each box represent mean of $|\alpha|$ plus and minus one standard deviation for the data in the corresponding range of S values.

The mean spot diameter was 170 μrad in the horizontal axis and 160 μrad in the vertical. No substantial spreading because of turbulence is observed. The plot of spot size as a function of signal power in Fig. 27 shows no dependence of spot size on signal level except at very low signals.

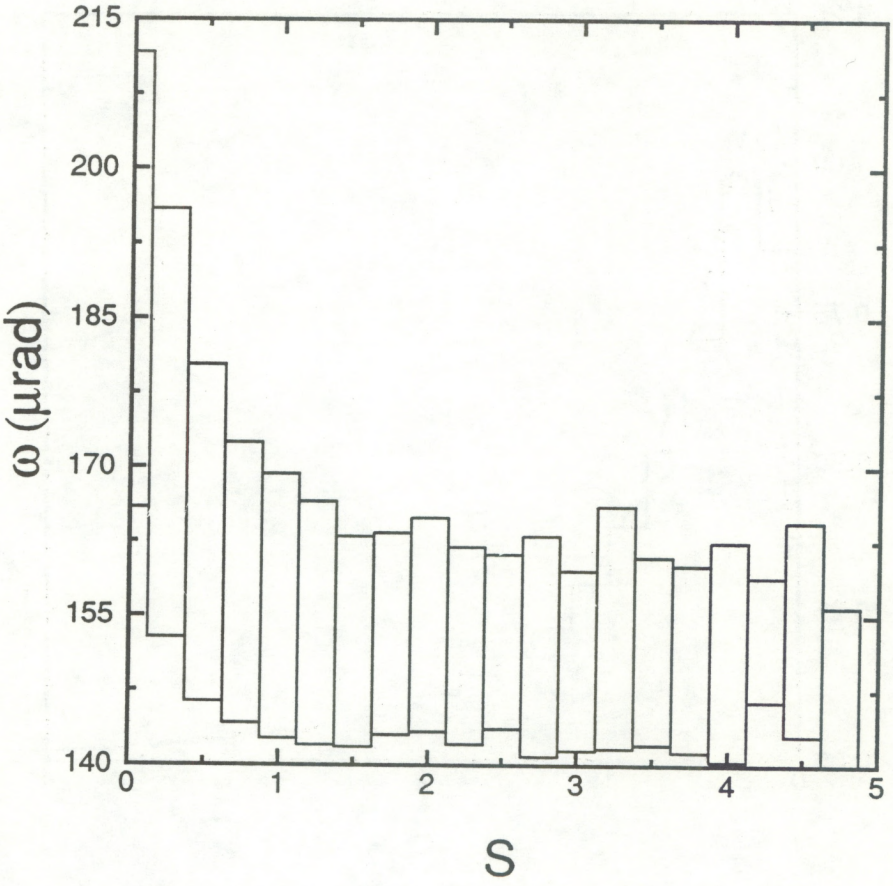

Fig. 27. Root-mean-square average of the horizonal and vertical spot diameters ω as a function of normalized signal power S. Top and bottom of each box represent mean of ω plus and minus one standard deviation for the data in the data in the corresponding range of S values.

Run 32 was obtained on the 500-m path using a 3-mm aperture. The turbulence parameters were $C_n^2 = 2.9 \pm 0.6 \times 10^{-13}$ $m^{-2/3}$ and $l_o = 7.1 \pm 0.5$ mm. The signals were very nearly log normal (Fig. 28), with a variance of 1.7 on each array and a correlation coefficient of 0.9986.

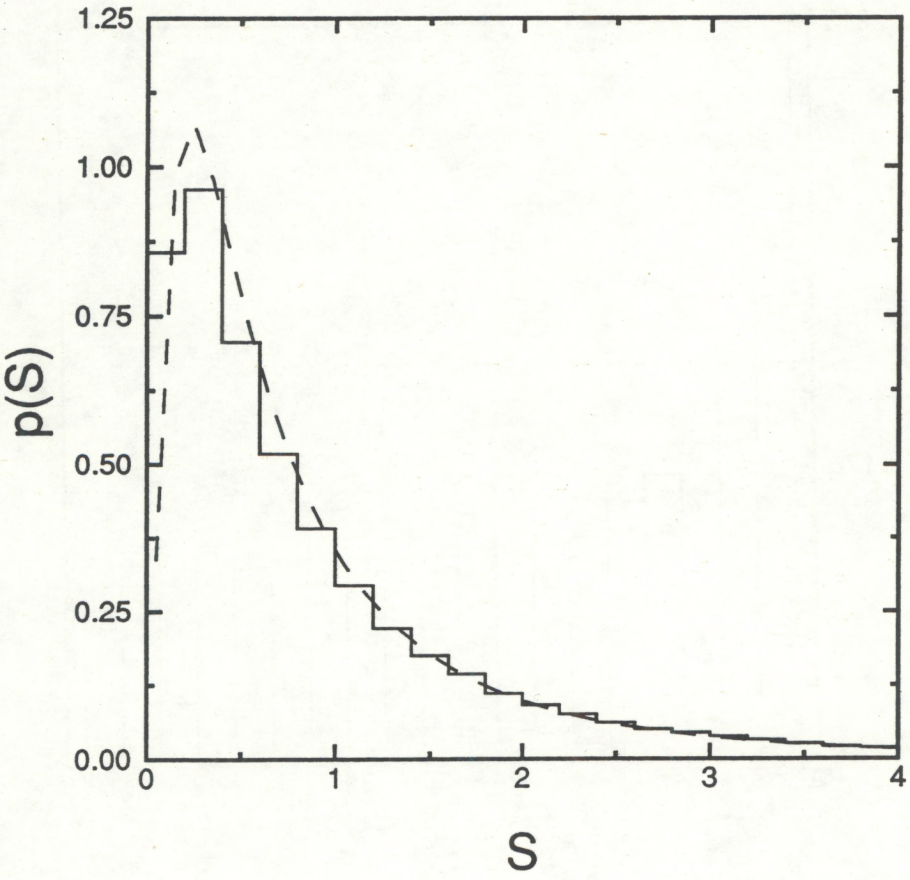

Fig. 28. Probability density function p(S) of normalized signal power *S* from vertical array with 3-mm aperture and 100-m path. Solid line is measured histogram and dashed line is a lognormal density function with variance of 1.7.

The displacement statistics for this case also show the effects of noise. The measured horizontal and vertical variances of 3.2×10^{-8} and 2.2×10^{-8} are much larger than the predicted value of 1.5×10^{-9}. The probability density function is not Rayleigh because of a substantial number of large displacements (Fig. 29). As before, the displacements are large when the signal power is low (Fig. 30). Despite this, the plot in Fig. 30 shows no dependence of displacement on signal level for signals above the mean value.

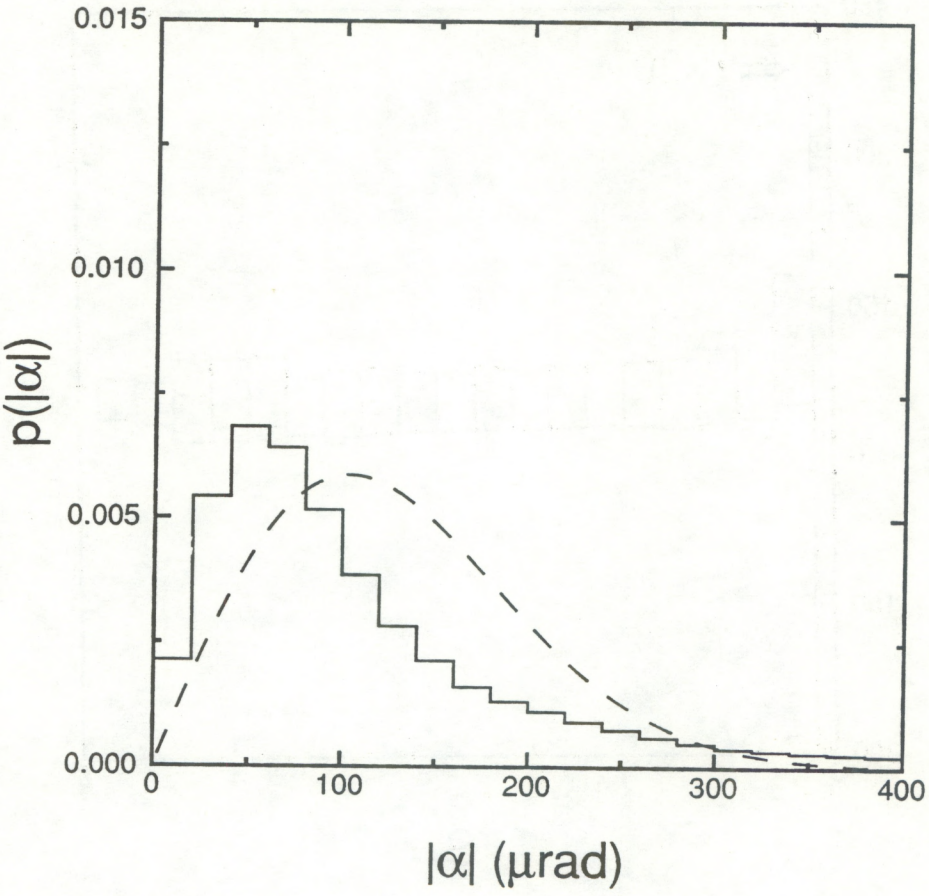

Fig. 29. Probability density function p(|α|) of magnitude of angular displacement |α| using 3-mm aperture and 100-m path. Solid line is measured histogram and dashed line is a Rayleigh density function with of 130 μrad.

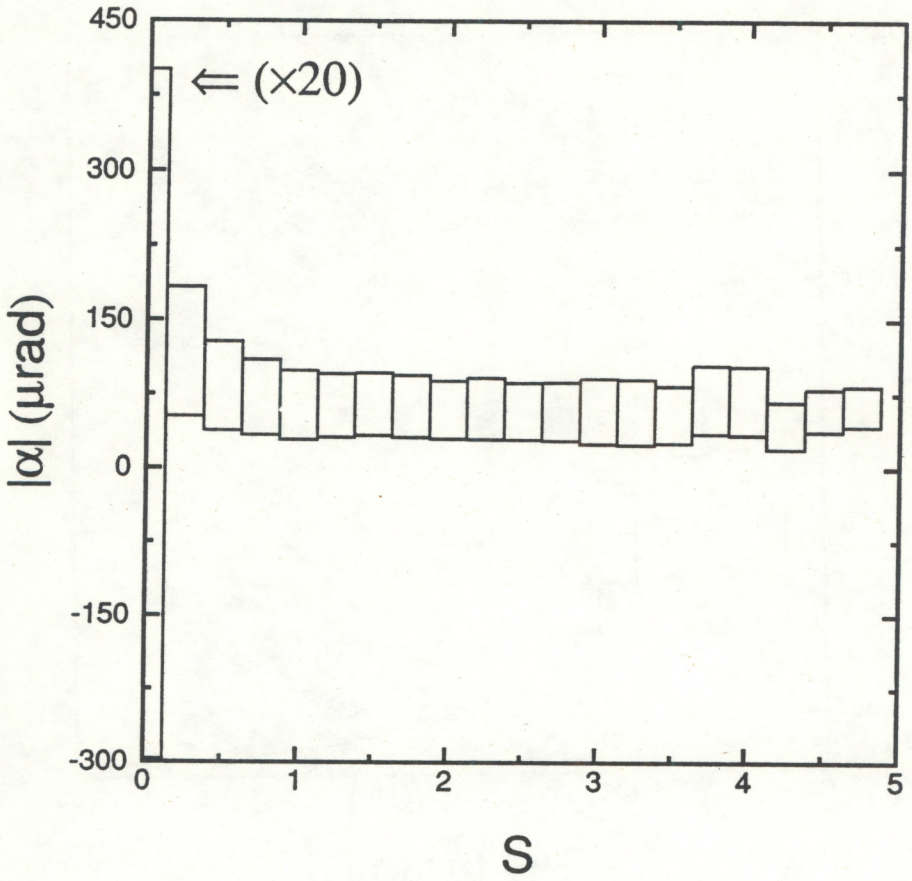

Fig. 30. Magnitude of angular displacement $|\alpha|$ as a function of normalized signal power S. Top and bottom of each box represent mean of $|\alpha|$ plus and minus one standard deviation for the data in the corresponding range of S values.

The mean spot diameter was 220 μrad in the horizontal axis and 230 μrad in the vertical; the spot is diffraction limited for this case as well. The plot of spot diameter as a function of signal level in Fig. 31 shows no dependence at signal levels above the mean.

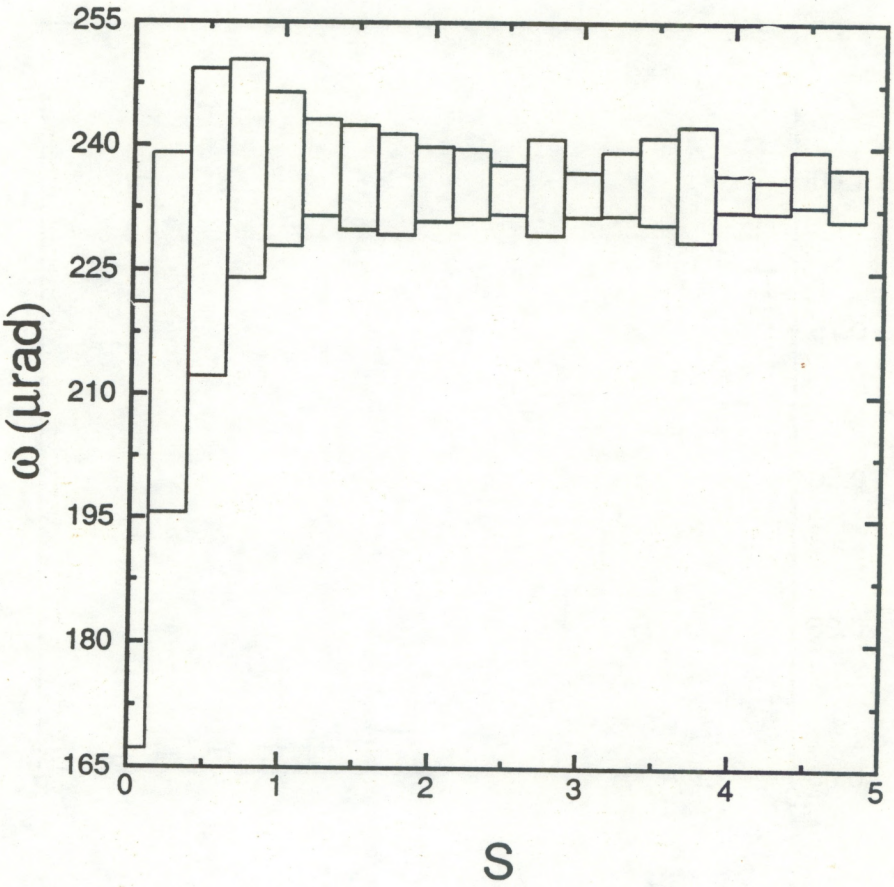

Fig. 31. Root-mean-square average of the horizontal and vertical spot diameters ω as a function of normalized signal power S. Top and bottom of each box represent mean of ω plus and minus one standard deviation for the data in the corresponding range of S values.

Runs 26, 27, 28, and 29 were taken over a 1000-m path. Runs 28 and 29 are discussed briefly; 26 and 27 are summarized in Appendix A.

Run 28 used the 7-mm aperture. Turbulence conditions during this run were $C_n^2 = 1.1 \pm 0.3 \times 10^{-13}$ $m^{-2/3}$ and $l_o = 7.7 \pm 0.5$ mm. The signal variance on each axis was 1.4 and the correlation coefficient was 0.9996. Figure 32 shows that the probability density of signal power was log normal.

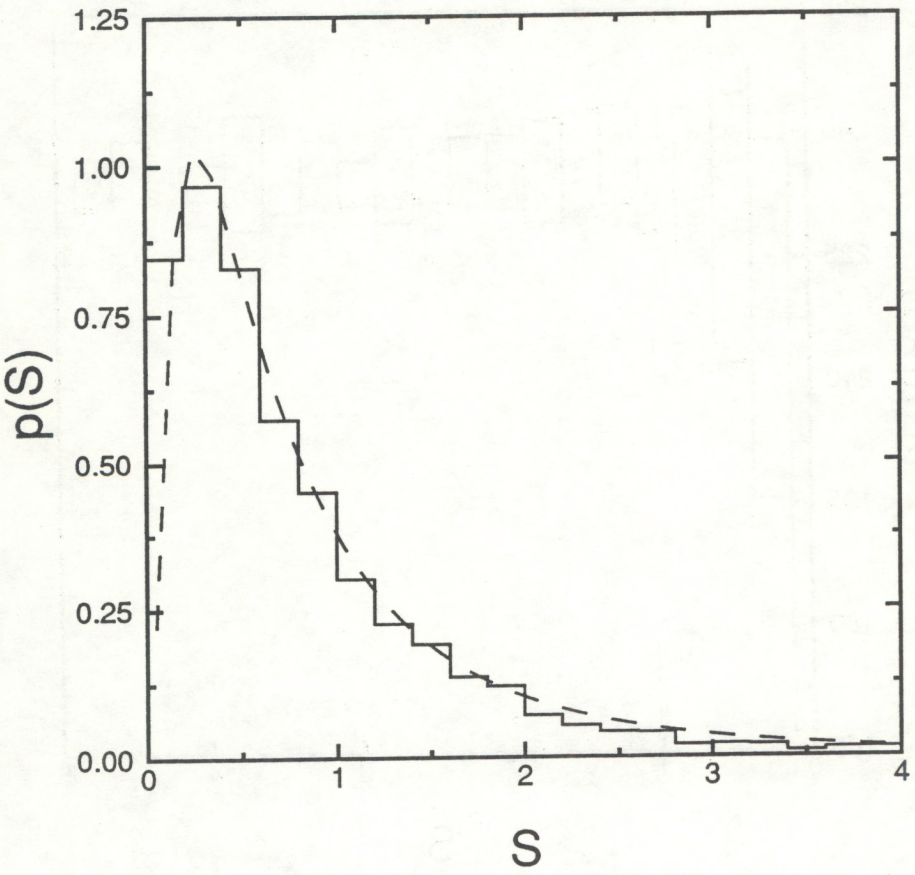

Fig. 32. Probability density function p(S) of normalized signal power *S* from vertical array with 7-mm aperture and 1000-m path. Solid line is measured histogram and dashed line is a lognormal density function with variance of 0.29.

The predicted variance of angular displacement for this case was 6.3×10^{-10} in each axis. The observed values were higher: 7.7×10^{-9} in the horizontal and 5.2×10^{-9} in the vertical. Figure 33 shows the deviation of the probability density function from Rayleigh because of the noise effects during deep fades. Figure 34 shows that neither the mean nor the variance of the displacement magnitude depend on signal power except at small signal levels.

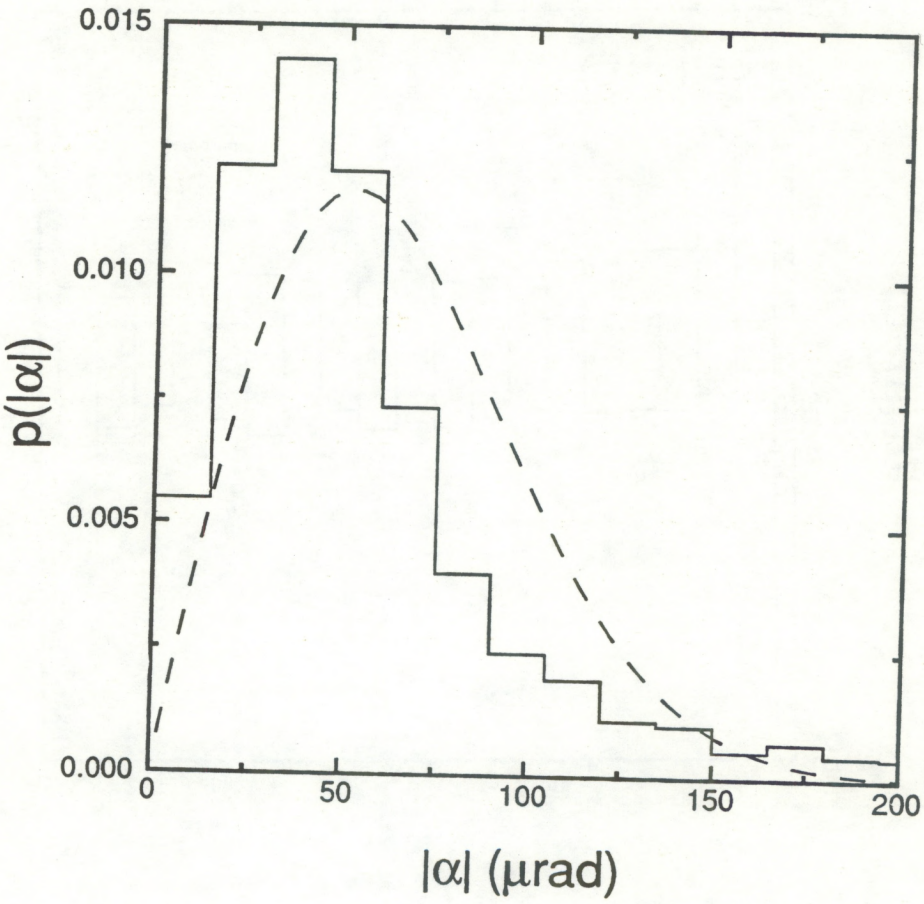

Fig. 33. Probability density function p(|α|) of magnitude of angular displacement |α| using 7-mm aperture and 1000-m path. Solid line is measured histogram and dashed line is a Rayleigh density function with mean of 65 μrad.

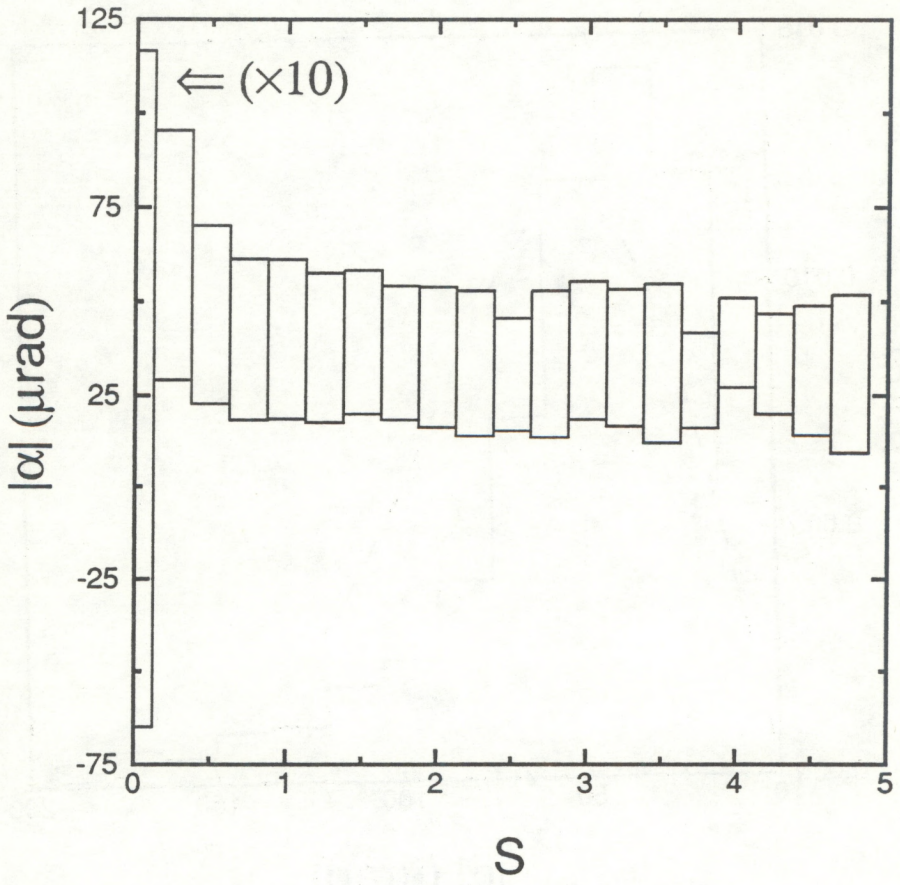

Fig. 34. Magnitude of angular displacement $|\alpha|$ as a function of normalized signal power S. Top and bottom of each box represent mean of $|\alpha|$ plus and minus one standard deviation for the data in the corresponding range of S values.

The mean spot diameter for this case was 180 μrad in each axis, and there is no significant broadening of the spot by the atmosphere. Figure 35 shows the spot size as a function of signal power; no dependence is seen except at small signal levels.

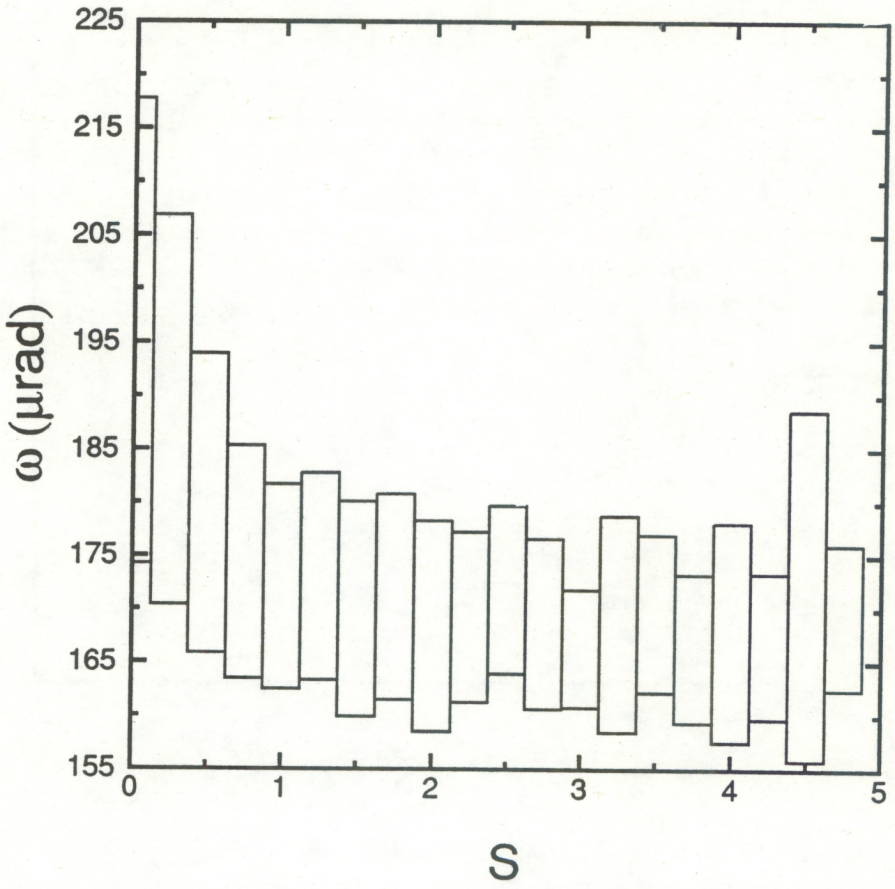

Fig. 35. Root-mean-square average of the horizontal and vertical spot diameters ω as a function of normalized signal power S. Top and bottom of each box represent mean of ω plus and minus one standard deviation for the data in the corresponding range of S values.

Run 29 was obtained using the 3-mm aperture. Turbulence conditions were $C_n^2 = 1.3 \pm 0.4 \times 10^{-13}$ $m^{-2/3}$ and $l_o = 7.4 \pm 0.6$ mm. The probability density of power was nearly log normal, although some slight deviation is apparent in Fig. 36. The variance on the horizontal array was 2.1 and on the vertical was 2.0. The correlation coefficient was 0.996.

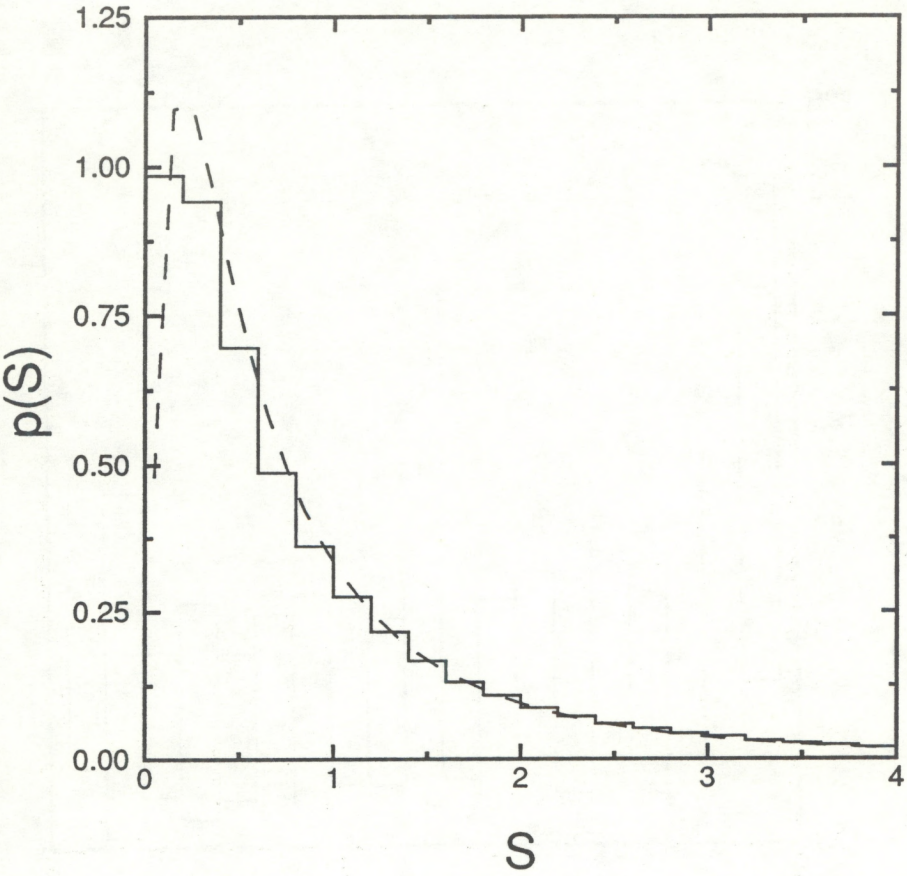

Fig. 36. Probability density function p(S) of normalized signal power *S* from vertical array with 3-mm aperture and 1000-m path. Solid line is measured histogram and dashed line is a lognormal density function with variance of 2.0.

The effects of noise on the displacement measurement are more pronounced when the 3-mm aperture is used at this path length than when the 7-mm aperture is used. The predicted variance on each axis was 9.6×10^{-10}. The actual observed values were 9.4×10^{-8} and 5.3×10^{-8}. As a result, the probability density function of the displacement magnitude in Fig. 37 shows significant deviation from Rayleigh. The plot of the displacement as a function of signal level in Fig. 38 shows very large displacements at small signal levels. At signal levels above the mean, no effect of signal level on displacement can be seen.

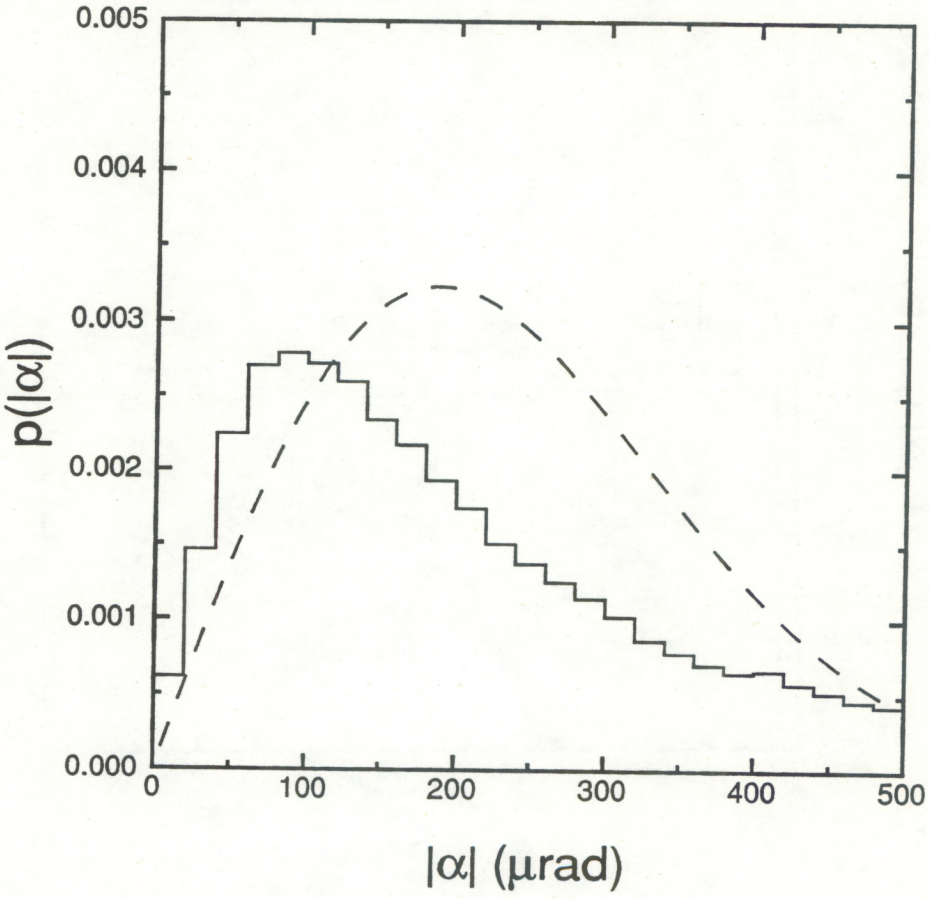

Fig. 37. Probability density function p(|α|) of magnitude of angular displacement |α| using 3-mm aperture and 1000-m path. Solid line is measured histogram and dashed line is Rayleigh density function with mean of 240 μrad.

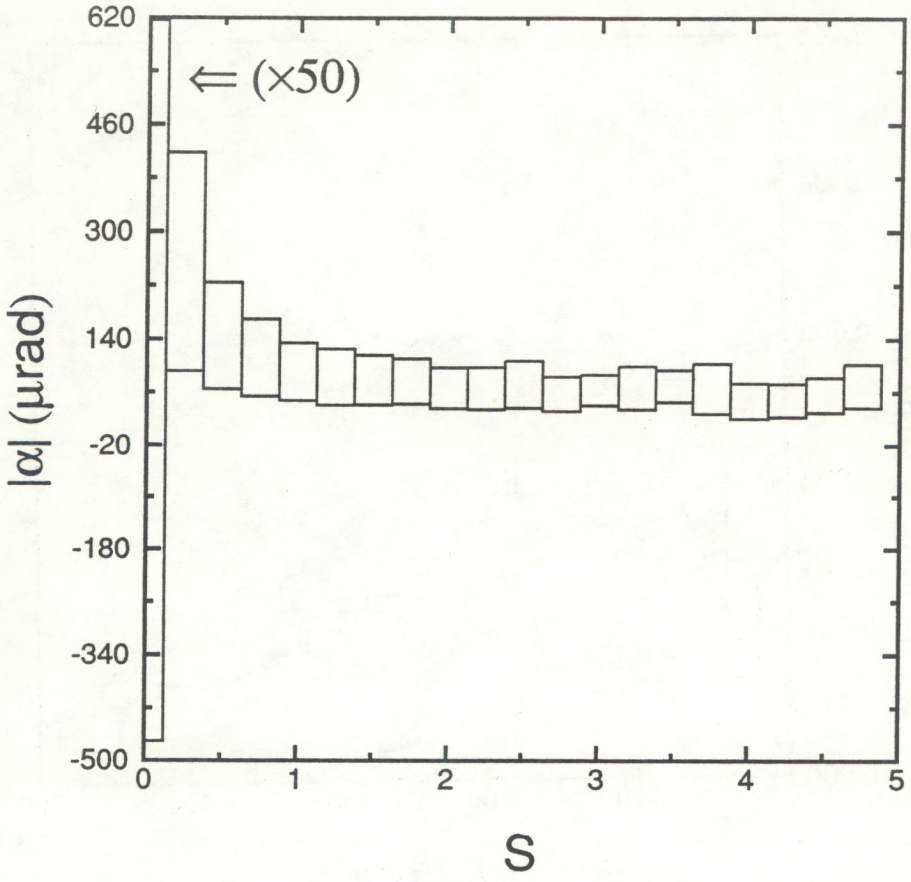

Fig. 38. Magnitude of angular displacement $|\alpha|$ as a function of normalized signal power S. Top and bottom of each box represent mean of $|\alpha|$ plus and minus one standard deviation for the data in the corresponding range of S values.

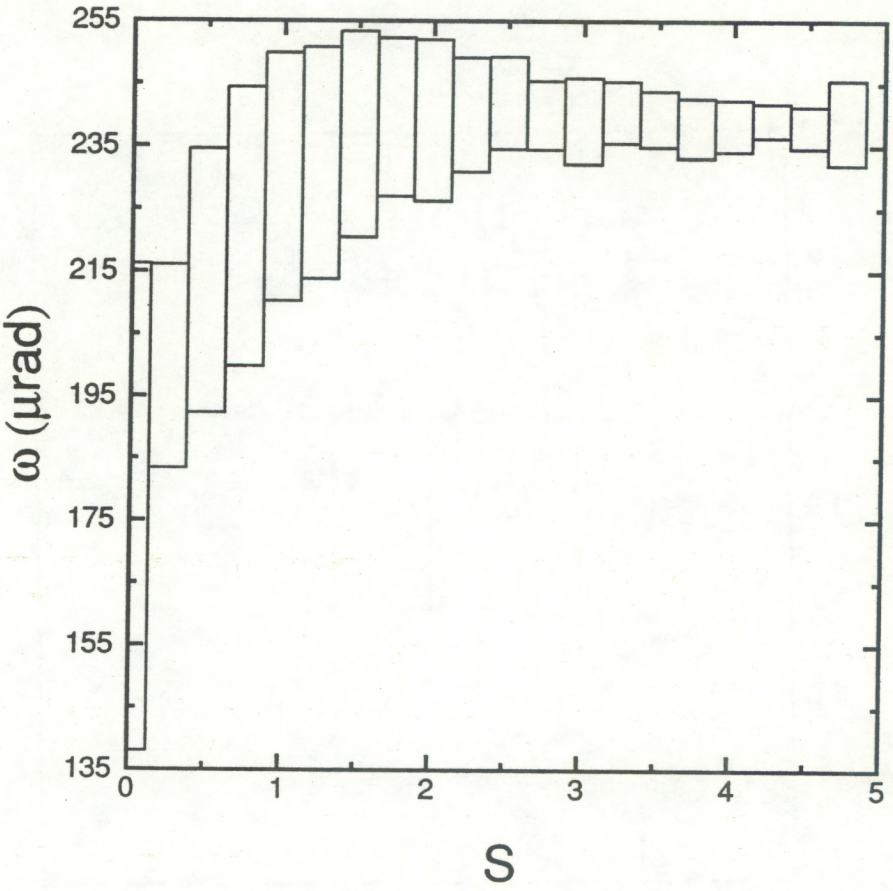

Fig. 39. Root-mean-square average of the horizontal and vertical spot diameters ω as a function of normalized signal power *S*. Top and bottom of each box represent mean of ω plus and minus one standard deviation for the data in the corresponding range of *S* values.

The measured spot sizes of 210 μrad (horizontal) and 220 μrad (vertical) imply that the spot size is still diffraction limited. A plot of the root-mean-square average of horizontal and vertical spot diameter as a function of signal level shows no dependence for signals larger than the mean value.

Runs 30 and 31 were taken on the nonuniform 600-m path. The 7-mm aperture was used in run 30. The normalized signal variance for this case was 0.062 and the correlation between the

two channels was 0.9985. The turbulence parameters could not be measured because of the nonuniformity of terrain. Figure 40 shows that the probability density function of signal power is log normal.

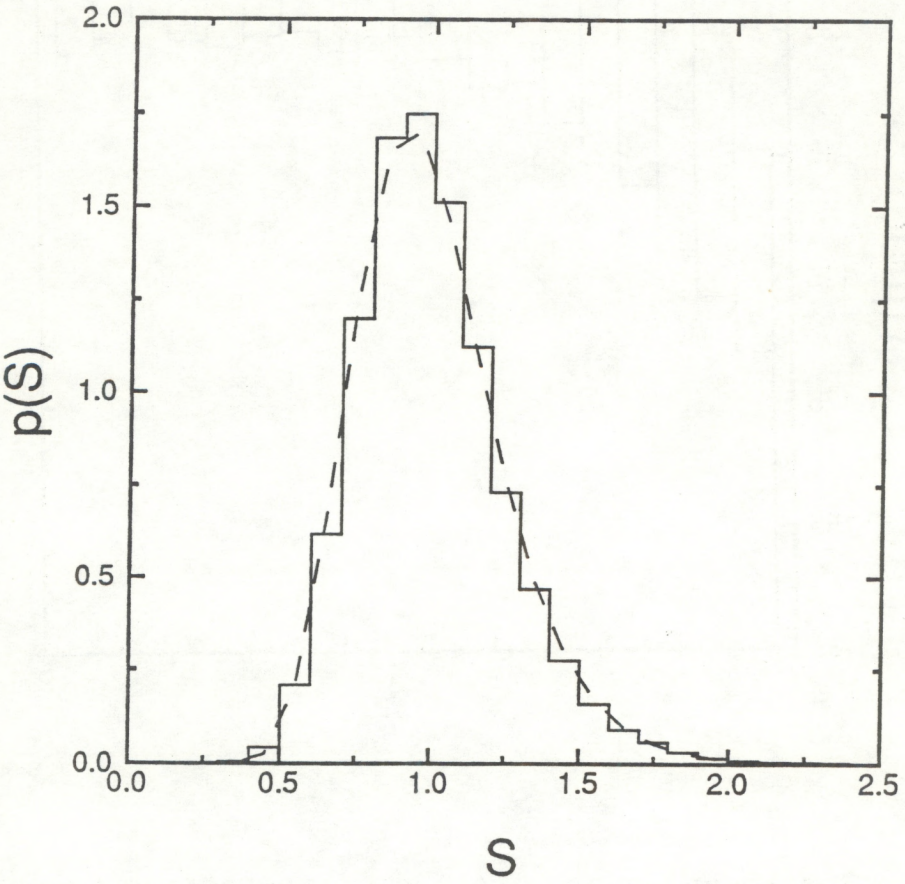

Fig. 40. Probability density function p(S) of normalized signal power *S* from vertical array with 7-mm aperture and 600-m path. Solid line is measured histogram and dashed line is a lognormal density function with variance of 0.062.

With few data points at very low signal levels, noise effects on the measured displacement magnitudes are small. Figure 41 shows that the probability density function of displacement magnitude is Rayleigh for this case. The displacement magnitude is independent of signal level for this case for signals above about a one-quarter of the mean value;

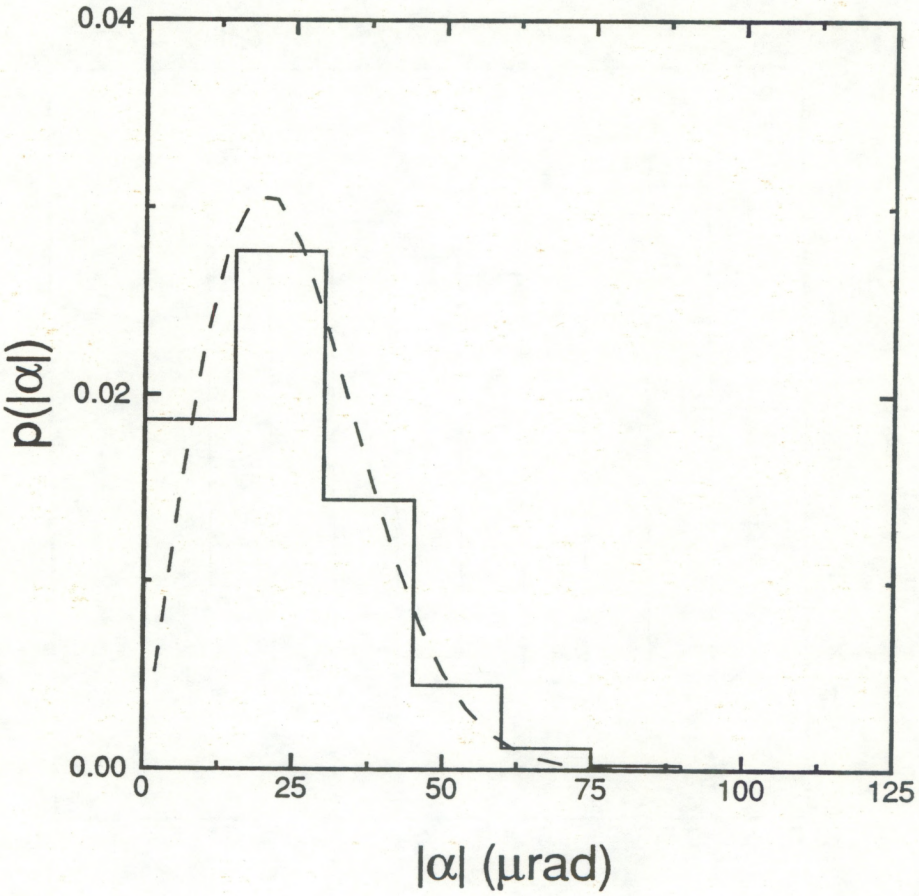

Fig. 41. Probability density function p(|α|) of magnitude of angular displacement |α| using 7-mm aperture and 600-m path. Solid line is measured histogram and dashed line is Rayleigh density function with mean of 25 μrad.

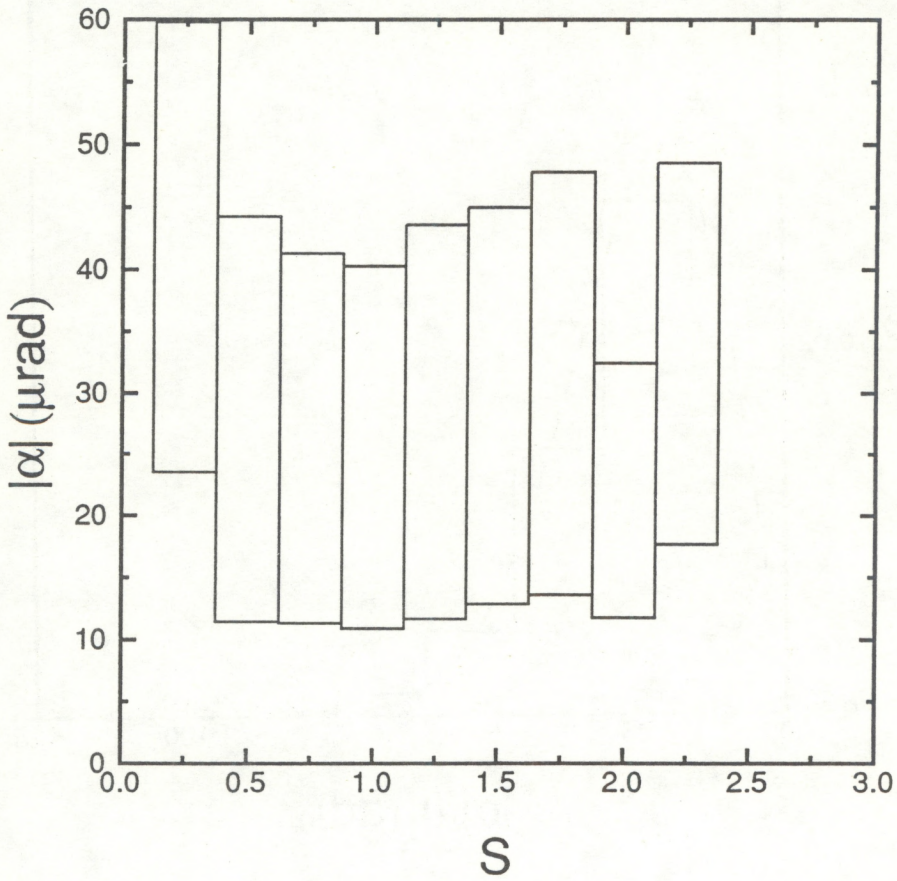

Fig. 42. Magnitude of angular displacement $|\alpha|$ as a function of normalized signal power S. Top and bottom of each box represent mean of $|\alpha|$ plus and minus one standard deviation for the data in the corresponding range of S values.

The mean spot diameters for this run were 180 μrad and 150 μrad and they are not affected by turbulence. A plot of the spot diameter as a function of signal power in Fig. 43 shows no dependence.

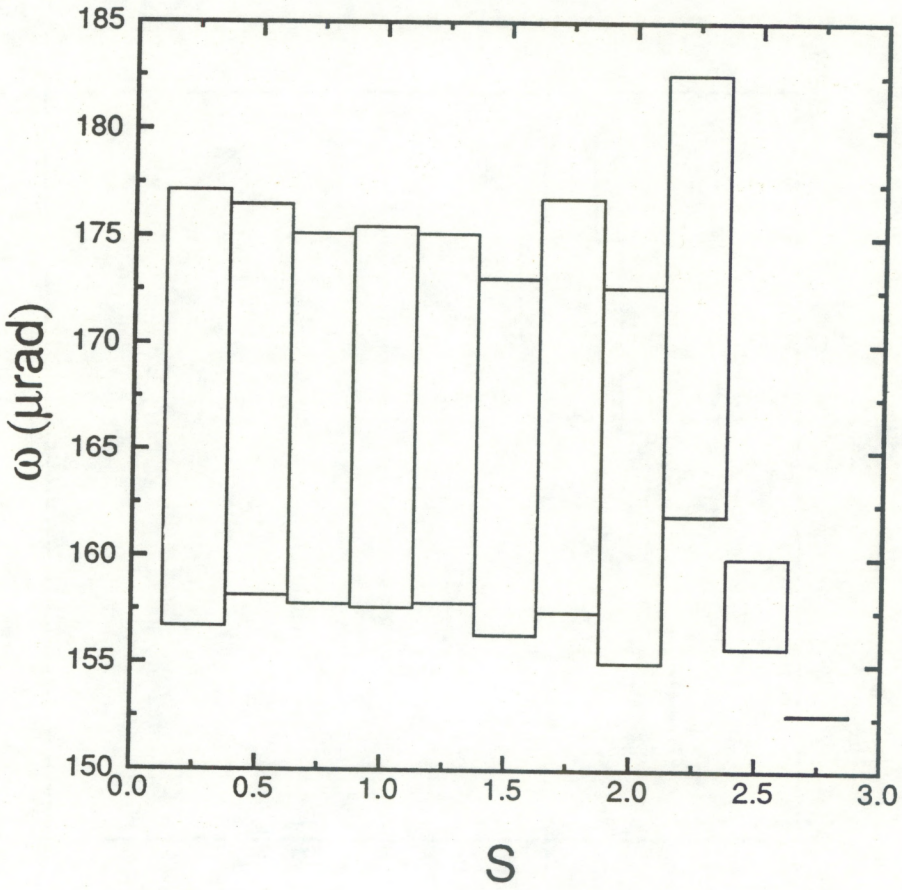

Fig. 43. Root-mean-square average of the horizontal and vertical spot diameters ω as a function of normalized signal power S. Top and bottom of each box represent mean of ω plus and minus one standard deviation for the data in the corresponding range of S values.

Run 31 was obtained using the 3-mm aperture. The normalized signal variance on the horizontal array was 0.081 and on the vertical array was 0.091. The correlation was lower at 0.96, suggesting that the noise was a larger fraction of the power fluctuations on this run than on others. The density function of signal fluctuations was log normal, as seen in Fig. 44.

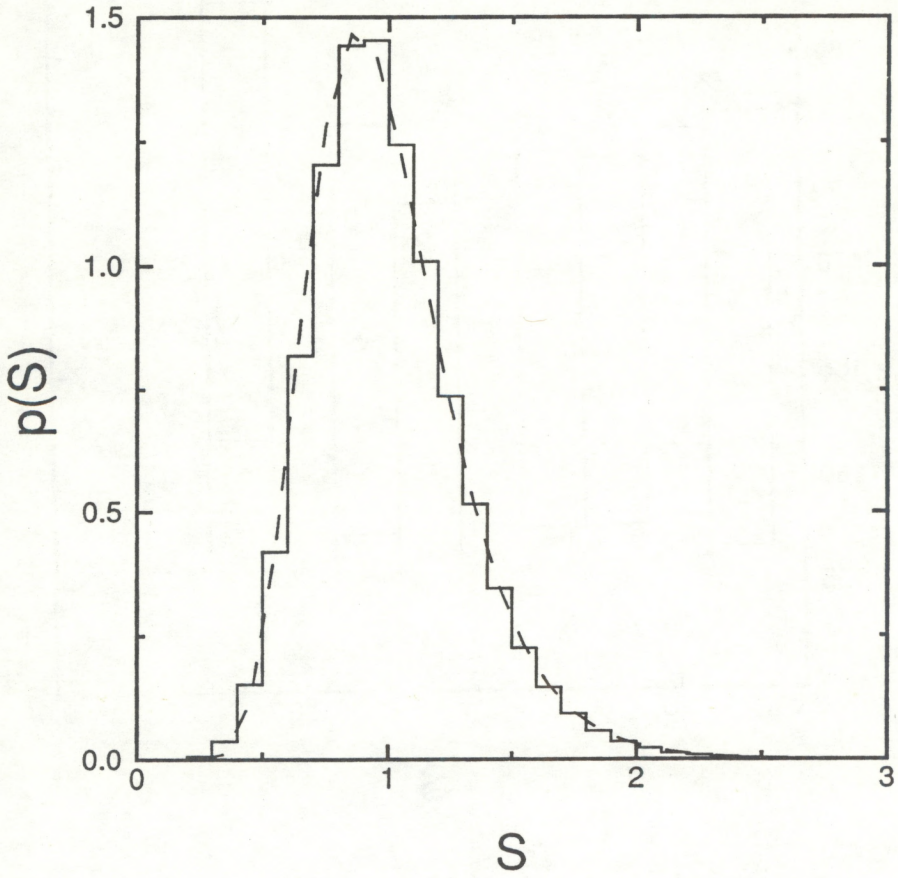

Fig. 44. Probability density function p(S) of normalized signal power S from vertical array with 3-mm aperture and 600-m path. Solid line is measured histogram and dashed line is a lognormal density function with variance of 0.091.

Figure 45 shows that the displacement magnitude has a nearly Rayleigh density function, despite the higher relative noise. Figure 46 shows large fluctuations in the estimated displacement at very low signal levels. However, there are few data points in the lowest bin, and the total statistics are not affected much.

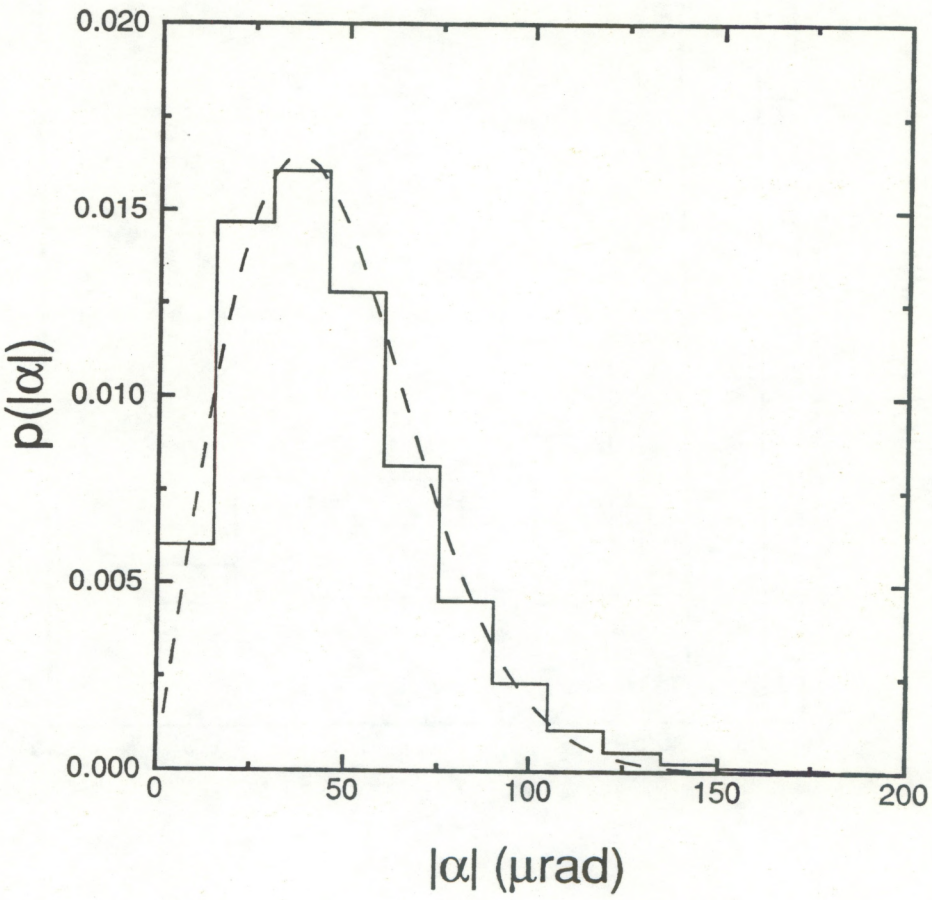

Fig. 45. Probability density function p(|α|) of magnitude of angular displacement |α| using 3-mm aperture and 600-m path. Solid line is measured histogram and dashed line is Rayleigh density function with mean of 46 μrad.

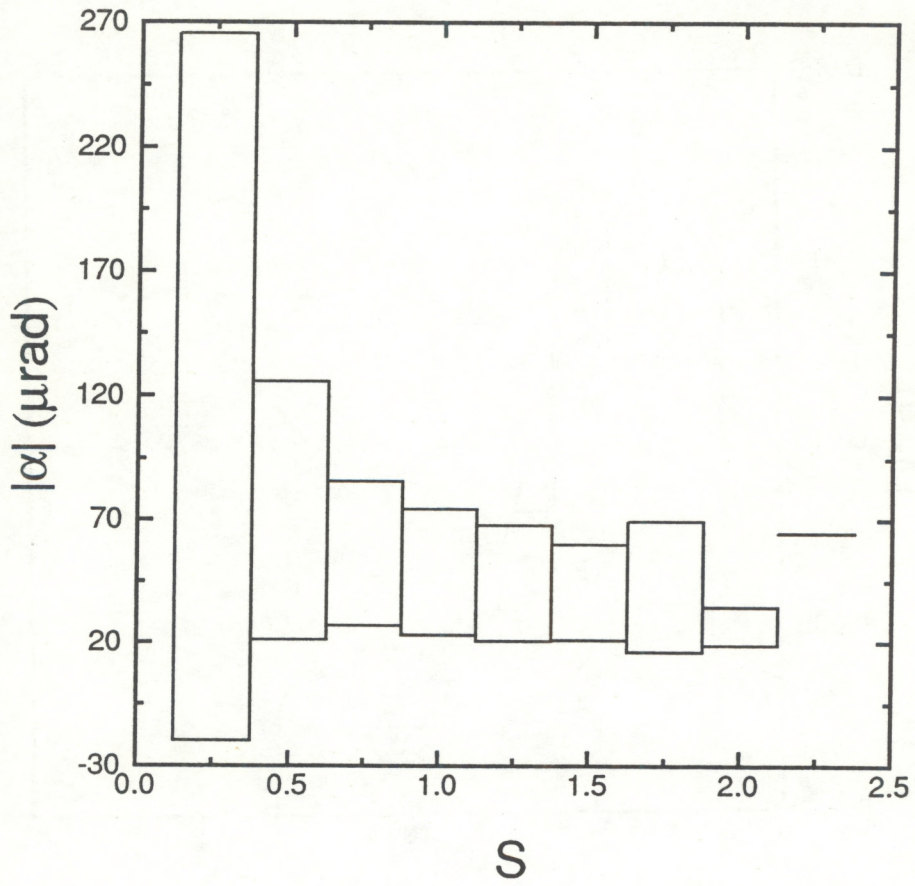

Fig. 46. Magnitude of angular displacement $|\alpha|$ as a function of normalized signal power S. Top and bottom of each box represent mean of $|\alpha|$ plus and minus one standard deviation for the data in the corresponding range of S values.

The mean spot diameter on each axis was 230 μrad and the receiver is diffraction limited. Figure 47 shows that there is no significant dependence of spot size on signal level except at low signal levels.

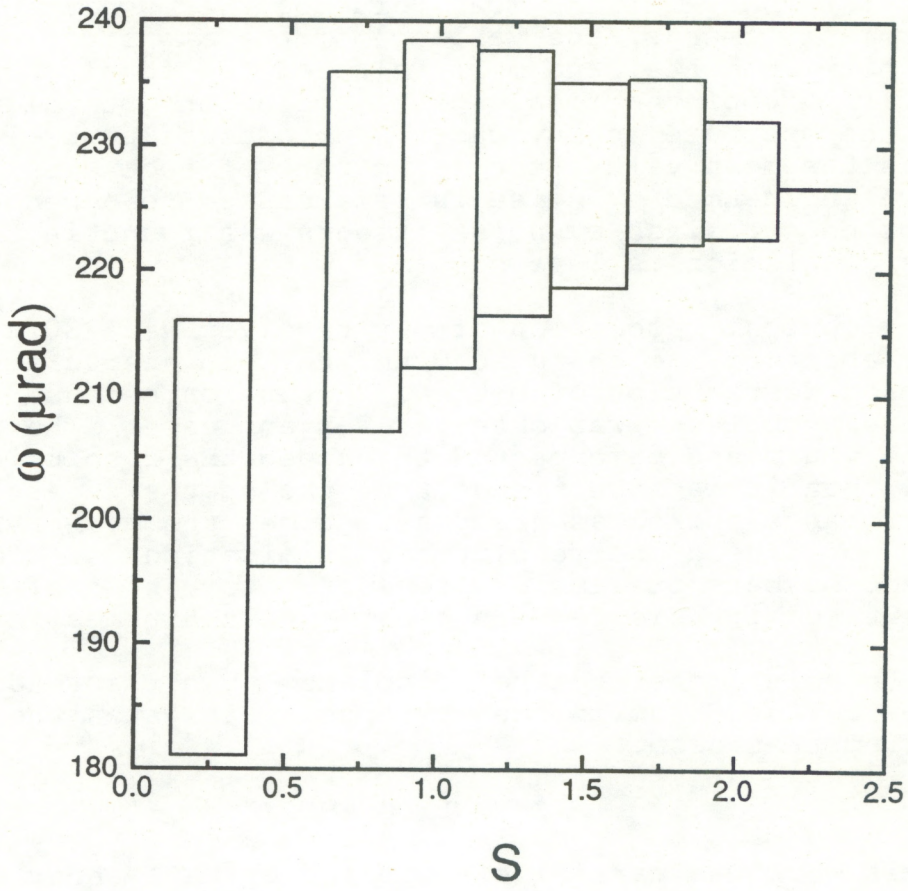

Fig. 47. Root-mean-square average of the horizontal and vertical spot diameters ω as a function of normalized signal power *S*. Top one bottom of each box represent mean of ω plus and minus are standard deviation for the data in the corresponding range of *S* values.

Several runs were taken on the 9-km path, but the signal-to-noise ratio was generally poor. Run 38 is included in Appendix A, but the results were generally too noisy to be useful. No evidence was obtained that the conclusions reached from the shorter paths would not also be valid for a 9-km path.

5. CONCLUSIONS

We have investigated a wide variety of propagation conditions, including weak path-integrated turbulence over short paths, weak path-integrated turbulence over long paths, and

strong path-integrated turbulence through 3- and 7-mm-diameter apertures. For optical power levels above the mean value, we found no dependence of the mean value of the magnitude of the angular displacements, the variance of the magnitude of the angular displacements, the mean value of the focal spot diameter, or the variance of the focal spot diameter on optical power through the aperture in any case. For optical power levels much less than the mean value, the estimators of spot displacement and size were influenced by noise in some cases; no dependence that could not be explained by noise effects was found in this region, but this conclusion is less secure.

The optical resolution of our receiver was 230 μrad with the 3-mm aperture and 180 μrad with the 7-mm aperture. No significant degradation of optical resolution because of refractive turbulence was observed for any case. The average spot size would not be expected to exceed the resolution of our receiver, but it is significant that the spot size associated with irradiance spikes as great as 5 times the mean irradiance also did not exceed the resolution. Limitations on digitizing very great numbers of samples prevents observation of the very rare events of irradiance much greater than 5 times its mean.

We conclude that neither displacement nor spreading of the spot from a laser beam in the atmosphere mitigates the ocular hazard from that beam.

ACKNOWLEDGMENTS

This work was partially supported by NASA under Order W-16,832. Ray Harrison provided the software and processed the data. Jim Wilson, Scott Abbott, and Duane Hazen designed and built the transmitter and receiver.

REFERENCES

Churnside, J.H., 1991: Aperture averaging factor for optical propagation through the turbulent atmosphere. *Appl. Opt.*, 30, in press.

Churnside, J.H. and R.J. Hill, 1987: Probability density of irradiance scintillations for strong path-integrated refractive turbulence. *J. Opt. Soc. Am. A, 4,* 727-733.

Churnside, J.H. and S.F. Clifford, 1987: Lognormal Rician probability-density function of optical scintillations in the turbulent atmosphere. *J. Opt. Soc. Am. A, 4,* 1923-1930.

Churnside, J.H. and R.J. Lataitis, 1987: Angle-of-arrival fluctuations of a reflected beam in atmospheric turbulence. *J. Opt. Soc. Am. A, 4,* 1264-1272.

Hill R.J., J.H. Churnside, and D.H. Sliney, 1987: Measured statistics of laser beam scintillation in strong refractive turbulence relevant to eye safety. *Health Phys., 53,* 639-647.

Hill R.J., and S.F. Clifford, 1978: Modified spectrum of atmospheric temperature fluctuations and its application to optical propagation. *J. Opt. Soc. Am., 68,* 892-899.

Lawrence R.S., and J.W. Strohbehn, 1970: A survey of clear-air propagation effects relevant to optical communications. *Proc. IEEE, 58,* 1523-1545.

Ochs G.R., W.D. Cartwright, and D.D. Russell, 1979: Optical C_n^2 Instrument Model II. NOAA Tech. Memo. ERL WPL-51 (available from National Technical Information Service, 5285 Port Royal Rd., Springfield, VA 22161; order number WPL51:PB 80-209000).

Ochs G.R., and R.J. Hill, 1985: Optical-scintillation method of measuring turbulence inner scale. *Appl. Opt., 24,* 2430-2432.

Shapiro S.H., 1978: Imaging and optical communication through atmospheric turbulence. In *Laser Beam Propagation in the Atmosphere;* Vol. 25 of Topics in Applied Physics, J.W. Strohbehn (Ed.) Springer-Verlag, New York.

Sliney D.H., and M.L. Wolbarsht, 1980: *Safety with Lasers and Other Optical Sources.* Plenum, New York.

APPENDIX A

This is a summary of the conditions and the results for each data run. In run 25, no data are available because of a misalignment of the receiver. In Runs 26, 27, 28, 29, 32, and 33, σ_s^2 is not available because of a lack of a valid saturation theory. In runs 30, 31, and 38, the turbulence parameters and quantities derived from them are not available because of the nonuniformity of the path. In run 34 and 35, the inner-scale meter was not operational.

RUN 20

Aperture Diameter	$D = 7$ mm
Path Length	$L = 100$ m
Turbulence Strength	$C_n^2 = 8.9 \times 10^{-13}$ $m^{-2/3}$
Inner Scale	$l_o = 5.7$ mm
Fresnel Zone Size	$\sqrt{\lambda L} = 9.1$ mm
Phase Coherence Length	$\rho_o = 8.5$ mm
Scintillation Index	$\beta = 0.22$
Signal Power	
Calculated Variance	$\sigma_s^2 = 0.18$
Measured Variance on Horizontal Array	$\sigma_{s_x}^2 = 0.17$
Measured Variance on Vertical Array	$\sigma_{s_y}^2 = 0.17$
Angle-of-Arrival	
Calibrated Single-Axis Standard Deviation	$\sigma_\alpha = 22$ μrad
Measured Standard Deviation on Horizontal Array	$\sigma_{\alpha_x} = 27$ μrad
Measured Standard Deviation on Vertical Array	$\sigma_{\alpha_y} = 29$ μrad
Average of Magnitude	$\lvert\overline{d}\rvert = 35$ μrad
Standard Deviation of Magnitude	$\sigma_{\lvert\alpha\rvert} = 19$ μrad
Correlation of Magnitude and Power	$r_\alpha = -3\%$
Spot Diameter	
Diffraction Limit	$W_D = 100$ μrad
Mean on Horizontal Array	$\overline{W}_x = 180$ μrad
Mean on Vertical Array	$\overline{W}_y = 180$ μrad
Standard Deviation on Horizontal Array	$\sigma_{W_x} = 13$ μrad
Standard Deviation on Vertical Array	$\sigma_{W_y} = 12$ μrad

RUN 21

Aperture Diameter	D	3 mm
Path Length	L	100 m
Turbulence Strength	C_n^2	9.4×10^{-13} $m^{-2/3}$
Inner Scale	l_o	5.9 mm
Fresnel Zone Size	$\sqrt{\lambda L}$	9.1 mm
Phase Coherence Length	ρ_o	8.2 mm
Scintillation Index	β	0.23
Signal Power		
Calculated Variance	σ_s^2	0.22
Measured Variance on Horizontal Array	$\sigma_{s_x}^2$	0.29
Measured Variance on Vertical Array	$\sigma_{s_y}^2$	0.29
Angle-of-Arrival		
Calibrated Single-Axis Standard Deviation	σ_α	27 μrad
Measured Standard Deviation on Horizontal Array	σ_{α_x}	49 μrad
Measured Standard Deviation on Vertical Array	σ_{α_y}	46 μrad
Average of Magnitude	$\lvert\bar{d}\rvert$	54 μrad
Standard Deviation of Magnitude	$\sigma_{\lvert\alpha\rvert}$	39 μrad
Correlation of Magnitude and Power	r_α	-37%
Spot Diameter		
Diffraction Limit	W_D	240 μrad
Mean on Horizontal Array	$\bar{w}_x$	230 μrad
Mean on Vertical Array	$\bar{w}_y$	240 μrad
Standard Deviation on Horizontal Array	σ_{w_x}	16 μrad
Standard Deviation on Vertical Array	σ_{w_y}	19 μrad

RUN 22

Aperture Diameter	D = 7	mm
Path Length	L = 250	m
Turbulence Strength	C_n^2 = 8.5 x 10^{-13}	
Inner Scale	l_o = 5.5	mm
Fresnel Zone Size	$\sqrt{\lambda L}$ = 1.4	mm
Phase Coherence Length	ρ_o = 5.1	mm
Scintillation Index	β = 1.1	
Signal Power		
Calculated Variance	σ_s^2 = 1.1	
Measured Variance on Horizontal Array	$\sigma_{s_x}^2$ = 1.3	
Measured Variance on Vertical Array	$\sigma_{s_y}^2$ = 1.3	
Angle-of-Arrival		
Calibrated Single-Axis Standard Deviation	σ_α = 34	μrad
Measured Standard Deviation on Horizontal Array	σ_{α_x} = 61	μrad
Measured Standard Deviation on Vertical Array	σ_{α_y} = 67	μrad
Average of Magnitude	$\lvert\bar{d}\rvert$ = 67	μrad
Standard Deviation of Magnitude	$\sigma_{\lvert\alpha\rvert}$ = 58	μrad
Correlation of Magnitude and Power	r_α = -16%	
Spot Diameter		
Diffraction Limit	$\bar{W}_D$ = 100	μrad
Mean on Horizontal Array	$\bar{W}_x$ = 170	μrad
Mean on Vertical Array	$\bar{W}_y$ = 170	μrad
Standard Deviation on Horizontal Array	σ_{W_x} = 27	μrad
Standard Deviation on Vertical Array	σ_{W_y} = 29	μrad

RUN 23

Aperture Diameter	$D = 3$ mm
Path Length	$L = 250$ m
Turbulence Strength	$C_n^2 = 8.3 \times 10^{-13}$ $m^{-2/3}$
Inner Scale	$l_o = 5.7$ mm
Fresnel Zone Size	$\sqrt{\lambda L} = 1.4$ mm
Phase Coherence Length	$\rho_o = 5.2$ mm
Scintillation Index	$\beta = 1.1$
Signal Power	
Calculated Variance	$\sigma_s^2 = 1.1$
Measured Variance on Horizontal Array	$\sigma_{s_x}^2 = 1.2$
Measured Variance on Vertical Array	$\sigma_{s_y}^2 = 1.2$
Angle-of-Arrival	
Calibrated Single-Axis Standard Deviation	$\sigma_\alpha = 39$ µrad
Measured Standard Deviation on Horizontal Array	$\sigma_{\alpha_x} = 160$ µrad
Measured Standard Deviation on Vertical Array	$\sigma_{\alpha_y} = 170$ µrad
Average of Magnitude	$\lvert\bar{d}\rvert = 130$ µrad
Standard Deviation of Magnitude	$\sigma_{\lvert\alpha\rvert} = 190$ µrad
Correlation of Magnitude and Power	$r_\alpha = -30\%$
Spot Diameter	
Diffraction Limit	$W_D = 240$ µrad
Mean on Horizontal Array	$\bar{w}_x = 220$ µrad
Mean on Vertical Array	$\bar{w}_y = 230$ µrad
Standard Deviation on Horizontal Array	$\sigma_{w_x} = 25$ µrad
Standard Deviation on Vertical Array	$\sigma_{w_y} = 30$ µrad

RUN 24

Aperture Diameter	D	= 7	mm
Path Length	L	= 500	m
Turbulence Strength	C_n^2	= 4.2×10^{-13}	$m^{-2/3}$
Inner Scale	l_o	= 6.5	mm
Fresnel Zone Size	$\sqrt{\lambda L}$	= 2.0	mm
Phase Coherence Length	ρ_o	= 5.3	mm
Scintillation Index	β	= 2.0	
Signal Power			
Calculated Variance	σ_s^2	= 2.0	
Measured Variance on Horizontal Array	$\sigma_{s_x}^2$	= 2.1	
Measured Variance on Vertical Array	$\sigma_{s_y}^2$	= 2.1	
Angle-of-Arrival			
Calibrated Single-Axis Standard Deviation	σ_α	= 33	μrad
Measured Standard Deviation on Horizontal Array	σ_{α_x}	= 120	μrad
Measured Standard Deviation on Vertical Array	σ_{α_y}	= 120	μrad
Average of Magnitude	$\lvert\vec{d}\rvert$	= 99	μrad
Standard Deviation of Magnitude	$\sigma_{\lvert\alpha\rvert}$	= 130	μrad
Correlation of Magnitude and Power	r_α	= -21%	
Spot Diameter			
Diffraction Limit	W_D	= 100	μrad
Mean on Horizontal Array	$\overline{W}_x$	= 190	μrad
Mean on Vertical Array	$\overline{W}_y$	= 200	μrad
Standard Deviation on Horizontal Array	σ_{W_x}	= 26	μrad
Standard Deviation on Vertical Array	σ_{W_y}	= 27	μrad

RUN 25

Aperture Diameter	$D = 3$ mm
Path Length	$L = 500$ m
Turbulence Strength	$C_n^2 = 3.6 \times 10^{-13}$
Inner Scale	$l_o = 6.7$ mm
Fresnel Zone Size	$\sqrt{\lambda L} = 2.0$ mm
Phase Coherence Length	$\rho_o = 5.7$ mm
Scintillation Index	$\beta = 1.7$
Signal Power	
Calculated Variance	$\sigma_s^2 =$
Measured Variance on Horizontal Array	$\sigma_{s_x}^2 =$
Measured Variance on Vertical Array	$\sigma_{s_y}^2 =$
Angle-of-Arrival	
Calibrated Single-Axis Standard Deviation	$\sigma_\alpha = 36$ μrad
Measured Standard Deviation on Horizontal Array	$\sigma_{\alpha_x} =$
Measured Standard Deviation on Vertical Array	$\sigma_{\alpha_y} =$
Average of Magnitude	$\lvert\bar{\alpha}\rvert =$
Standard Deviation of Magnitude	$\sigma_{\lvert\alpha\rvert} =$
Correlation of Magnitude and Power	$r_\alpha =$
Spot Diameter	
Diffraction Limit	$W_D =$
Mean on Horizontal Array	$\bar{w}_x =$
Mean on Vertical Array	$\bar{w}_y =$
Standard Deviation on Horizontal Array	$\sigma_{w_x} =$
Standard Deviation on Vertical Array	$\sigma_{w_y} =$

RUN 26

Aperture Diameter	$D = 7$ mm
Path Length	$L = 1$ km
Turbulence Strength	$C_n^2 = 2.1 \times 10^{-13}$
Inner Scale	$l_o = 6.3$ mm
Fresnel Zone Size	$\sqrt{\lambda L} = 2.9$ cm
Phase Coherence Length	$\rho_o = 5.2$ mm
Scintillation Index	$\beta = 3.6$
Signal Power	
Calculated Variance	$\sigma_s^2 =$
Measured Variance on Horizontal Array	$\sigma_{s_x}^2 = 2.9$
Measured Variance on Vertical Array	$\sigma_{s_y}^2 = 2.9$
Angle-of-Arrival	
Calibrated Single-Axis Standard Deviation	$\sigma_\alpha = 34$ μrad
Measured Standard Deviation on Horizontal Array	$\sigma_{\alpha_x} = 180$ μrad
Measured Standard Deviation on Vertical Array	$\sigma_{\alpha_y} = 150$ μrad
Average of Magnitude	$\lvert\overline{d}\rvert = 130$ μrad
Standard Deviation of Magnitude	$\sigma_{\lvert\alpha\rvert} = 190$ μrad
Correlation of Magnitude and Power	$r_\alpha = -22\%$
Spot Diameter	
Diffraction Limit	$W_D = 100$ μrad
Mean on Horizontal Array	$\overline{w}_x = 190$ μrad
Mean on Vertical Array	$\overline{w}_y = 200$ μrad
Standard Deviation on Horizontal Array	$\sigma_{w_x} = 25$ μrad
Standard Deviation on Vertical Array	$\sigma_{w_y} = 26$ μrad

RUN 27

Aperture Diameter	D	= 3	mm
Path Length	L	= 1	km
Turbulence Strength	C_n^2	= 6.9 x 10^{-14}	
Inner Scale	l_o	= 7.1	mm
Fresnel Zone Size	$\sqrt{\lambda L}$	= 2.9	mm
Phase Coherence Length	ρ_o	= 9.9	mm
Scintillation Index	β	= 1.2	
Signal Power			
Calculated Variance	σ_s^2	=	
Measured Variance on Horizontal Array	$\sigma_{s_x}^2$	= 1.1	
Measured Variance on Vertical Array	$\sigma_{s_y}^2$	= 1.0	
Angle-of-Arrival			
Calibrated Single-Axis Standard Deviation	σ_α	= 23	μrad
Measured Standard Deviation on Horizontal Array	σ_{α_x}	= 290	μrad
Measured Standard Deviation on Vertical Array	σ_{α_y}	= 200	μrad
Average of Magnitude	$\lvert\overline{d}\rvert$	= 220	μrad
Standard Deviation of Magnitude	$\sigma_{\lvert\alpha\rvert}$	= 270	μrad
Correlation of Magnitude and Power	r_α	= -38%	
Spot Diameter			
Diffraction Limit	W_D	= 240	μrad
Mean on Horizontal Array	$\overline{w}_x$	= 210	μrad
Mean on Vertical Array	$\overline{w}_y$	= 220	μrad
Standard Deviation on Horizontal Array	σ_{w_x}	= 25	μrad
Standard Deviation on Vertical Array	σ_{w_y}	= 32	μrad

RUN 28

Aperture Diameter	D	= 7	mm
Path Length	L	= 1	km
Turbulence Strength	C_n^2	= 1.1 x 10^{-13}	
Inner Scale	l_o	= 7.7	mm
Fresnel Zone Size	$\sqrt{\lambda L}$	= 2.9	cm
Phase Coherence Length	ρ_o	= 7.5	mm
Scintillation Index	β	= 1.9	
Signal Power			
Calculated Variance	σ_s^2	=	
Measured Variance on Horizontal Array	$\sigma_{s_x}^2$	= 1.4	
Measured Variance on Vertical Array	$\sigma_{s_y}^2$	= 1.4	
Angle-of-Arrival			
Calibrated Single-Axis Standard Deviation	σ_α	= 25	μrad
Measured Standard Deviation on Horizontal Array	σ_{α_x}	= 88	μrad
Measured Standard Deviation on Vertical Array	σ_{α_y}	= 72	μrad
Average of Magnitude	$\lvert\overline{d}\rvert$	= 65	μrad
Standard Deviation of Magnitude	$\sigma_{\lvert\alpha\rvert}$	= 92	μrad
Correlation of Magnitude and Power	r_α	= -22%	
Spot Diameter			
Diffraction Limit	W_D	= 100	μrad
Mean on Horizontal Array	$\overline{w}_x$	= 180	μrad
Mean on Vertical Array	$\overline{w}_y$	= 180	μrad
Standard Deviation on Horizontal Array	σ_{w_x}	= 21	μrad
Standard Deviation on Vertical Array	σ_{w_y}	= 22	μrad

RUN 29

Aperture Diameter	$D = 3$ mm
Path Length	$L = 1$ km
Turbulence Strength	$C_n^2 = 1.3 \times 10^{-13}$ $m^{-2/3}$
Inner Scale	$l_o = 7.4$ mm
Fresnel Zone Size	$\sqrt{\lambda L} = 2.9$ mm
Phase Coherence Length	$\rho_o = 6.8$ mm
Scintillation Index	$\beta = 2.2$
Signal Power	
Calculated Variance	$\sigma_s^2 =$
Measured Variance on Horizontal Array	$\sigma_{s_x}^2 = 2.1$
Measured Variance on Vertical Array	$\sigma_{s_y}^2 = 2.0$
Angle-of-Arrival	
Calibrated Single-Axis Standard Deviation	$\sigma_\alpha = 31$ μrad
Measured Standard Deviation on Horizontal Array	$\sigma_{\alpha_x} = 310$ μrad
Measured Standard Deviation on Vertical Array	$\sigma_{\alpha_y} = 230$ μrad
Average of Magnitude	$\lvert\overline{d}\rvert = 240$ μrad
Standard Deviation of Magnitude	$\sigma_{\lvert\alpha\rvert} = 300$ μrad
Correlation of Magnitude and Power	$r_\alpha = -32\%$
Spot Diameter	
Diffraction Limit	$W_D = 240$ μrad
Mean on Horizontal Array	$\overline{w}_x = 210$ μrad
Mean on Vertical Array	$\overline{w}_y = 220$ μrad
Standard Deviation on Horizontal Array	$\sigma_{w_x} = 26$ μrad
Standard Deviation on Vertical Array	$\sigma_{w_y} = 31$ μrad

RUN 30

Aperture Diameter	D	= 7	mm
Path Length	L	= 600	m
Turbulence Strength	C_n^2	=	
Inner Scale	l_o	=	
Fresnel Zone Size	$\sqrt{\lambda L}$	= 2.2	cm
Phase Coherence Length	ρ_o	=	
Scintillation Index	β	=	
Signal Power			
Calculated Variance	σ_s^2	=	
Measured Variance on Horizontal Array	$\sigma_{s_x}^2$	= 0.062	
Measured Variance on Vertical Array	$\sigma_{s_y}^2$	= 0.062	
Angle-of-Arrival			
Calibrated Single-Axis Standard Deviation	σ_α	=	μrad
Measured Standard Deviation on Horizontal Array	σ_{α_x}	= 18	μrad
Measured Standard Deviation on Vertical Array	σ_{α_y}	= 22	μrad
Average of Magnitude	$\lvert\bar{d}\rvert$	= 25	μrad
Standard Deviation of Magnitude	$\sigma_{\lvert\alpha\rvert}$	= 14	μrad
Correlation of Magnitude and Power	r_α	= -3%	
Spot Diameter			
Diffraction Limit	W_D	= 100	μrad
Mean on Horizontal Array	$\bar{W}_x$	= 180	μrad
Mean on Vertical Array	$\bar{W}_y$	= 150	μrad
Standard Deviation on Horizontal Array	σ_{W_x}	= 11	μrad
Standard Deviation on Vertical Array	σ_{W_y}	= 11	μrad

RUN 31

Aperture Diameter	D = 3 mm	
Path Length	L = 600 m	
Turbulence Strength	C_n^2 =	
Inner Scale	l_o =	
Fresnel Zone Size	$\sqrt{\lambda L}$ = 2.2 cm	
Phase Coherence Length	ρ_o =	
Scintillation Index	β =	
Signal Power		
Calculated Variance	σ_s^2 =	
Measured Variance on Horizontal Array	$\sigma_{s_x}^2$ = 0.081	
Measured Variance on Vertical Array	$\sigma_{s_y}^2$ = 0.091	
Angle-of-Arrival		
Calibrated Single-Axis Standard Deviation	σ_α =	
Measured Standard Deviation on Horizontal Array	σ_{α_x} = 37	μrad
Measured Standard Deviation on Vertical Array	σ_{α_y} = 39	μrad
Average of Magnitude	$\lvert\overline{d}\rvert$ = 46	μrad
Standard Deviation of Magnitude	$\sigma_{\lvert\alpha\rvert}$ = 27	μrad
Correlation of Magnitude and Power	r_α = -32%	
Spot Diameter		
Diffraction Limit	W_D = 240	μrad
Mean on Horizontal Array	$\overline{w}_x$ = 230	μrad
Mean on Vertical Array	$\overline{w}_y$ = 230	μrad
Standard Deviation on Horizontal Array	σ_{w_x} = 14	μrad
Standard Deviation on Vertical Array	σ_{w_y} = 18	μrad

RUN 32

Aperture Diameter	D = 3	mm
Path Length	L = 500	m
Turbulence Strength	C_n^2 = 2.9 x 10^{-13}	$m^{-2/3}$
Inner Scale	l_o = 7.1	mm
Fresnel Zone Size	$\sqrt{\lambda L}$ = 2.0	cm
Phase Coherence Length	ρ_o = 6.4	mm
Scintillation Index	β = 1.4	
Signal Power		
Calculated Variance	σ_s^2 =	
Measured Variance on Horizontal Array	$\sigma_{s_x}^2$ = 1.7	
Measured Variance on Vertical Array	$\sigma_{s_y}^2$ = 1.7	
Angle-of-Arrival		
Calibrated Single-Axis Standard Deviation	σ_α = 33	μrad
Measured Standard Deviation on Horizontal Array	σ_{α_x} = 180	μrad
Measured Standard Deviation on Vertical Array	σ_{α_y} = 150	μrad
Average of Magnitude	$\lvert\overline{d}\rvert$ = 130	μrad
Standard Deviation of Magnitude	$\sigma_{\lvert\alpha\rvert}$ = 190	μrad
Correlation of Magnitude and Power	r_α = -28%	
Spot Diameter		
Diffraction Limit	W_D = 240	μrad
Mean on Horizontal Array	$\overline{w}_x$ = 220	μrad
Mean on Vertical Array	$\overline{w}_y$ = 230	μrad
Standard Deviation on Horizontal Array	σ_{w_x} = 24	μrad
Standard Deviation on Vertical Array	σ_{w_y} = 29	μrad

RUN 33

Aperture Diameter	D	= 7	mm
Path Length	L	= 500	m
Turbulence Strength	C_n^2	= 4.1×10^{-13}	
Inner Scale	l_o	= 7.0	mm
Fresnel Zone Size	$\sqrt{\lambda L}$	= 2.0	cm
Phase Coherence Length	ρ_o	= 5.4	mm
Scintillation Index	β	= 1.9	
Signal Power			
Calculated Variance	σ_s^2	=	
Measured Variance on Horizontal Array	$\sigma_{s_x}^2$	= 1.5	
Measured Variance on Vertical Array	$\sigma_{s_y}^2$	= 1.4	
Angle-of-Arrival			
Calibrated Single-Axis Standard Deviation	σ_α	= 33	μrad
Measured Standard Deviation on Horizontal Array	σ_{α_x}	= 74	μrad
Measured Standard Deviation on Vertical Array	σ_{α_y}	= 94	μrad
Average of Magnitude	$\lvert\bar{d}\rvert$	= 73	μrad
Standard Deviation of Magnitude	$\sigma_{\lvert\alpha\rvert}$	= 95	μrad
Correlation of Magnitude and Power	r_α	= -23%	
Spot Diameter			
Diffraction Limit	W_D	= 100	μrad
Mean on Horizontal Array	$\bar{w}_x$	= 170	μrad
Mean on Vertical Array	$\bar{w}_y$	= 160	μrad
Standard Deviation on Horizontal Array	σ_{w_x}	= 25	μrad
Standard Deviation on Vertical Array	σ_{w_y}	= 31	μrad

RUN 34

Aperture Diameter	$D = 7$ mm
Path Length	$L = 250$ m
Turbulence Strength	$C_n^2 = 4.2 \times 10^{-13}$
Inner Scale	$l_o =$
Fresnel Zone Size	$\sqrt{\lambda L} = 1.4$ cm
Phase Coherence Length	$\rho_o =$
Scintillation Index	$\beta = 0.57$
Signal Power	
Calculated Variance	$\sigma_s^2 = 0.53$
Measured Variance on Horizontal Array	$\sigma_{s_x}^2 = 0.59$
Measured Variance on Vertical Array	$\sigma_{s_y}^2 = 0.59$
Angle-of-Arrival	
Calibrated Single-Axis Standard Deviation	$\sigma_\alpha =$
Measured Standard Deviation on Horizontal Array	$\sigma_{\alpha_x} = 32$ μrad
Measured Standard Deviation on Vertical Array	$\sigma_{\alpha_y} = 40$ μrad
Average of Magnitude	$\lvert\overline{d}\rvert = 44$ μrad
Standard Deviation of Magnitude	$\sigma_{\lvert\alpha\rvert} = 26$ μrad
Correlation of Magnitude and Power	$r_\alpha = -14\%$
Spot Diameter	
Diffraction Limit	$W_D = 100$ μrad
Mean on Horizontal Array	$\overline{w}_x = 170$ μrad
Mean on Vertical Array	$\overline{w}_y = 150$ μrad
Standard Deviation on Horizontal Array	$\sigma_{w_x} = 20$ μrad
Standard Deviation on Vertical Array	$\sigma_{w_y} = 22$ μrad

RUN 35

Aperture Diameter	D = 3 mm	
Path Length	L = 250 m	
Turbulence Strength	C_n^2 = 4.5×10^{-13}	
Inner Scale	l_o =	
Fresnel Zone Size	$\sqrt{\lambda L}$ = 1.4 cm	
Phase Coherence Length	ρ_o =	
Scintillation Index	β = 0.61	
Signal Power		
Calculated Variance	σ_s^2 = 0.60	
Measured Variance on Horizontal Array	$\sigma_{s_x}^2$ = 0.93	
Measured Variance on Vertical Array	$\sigma_{s_y}^2$ = 0.91	
Angle-of-Arrival		
Calibrated Single-Axis Standard Deviation	σ_α =	
Measured Standard Deviation on Horizontal Array	σ_{α_x} = 100	μrad
Measured Standard Deviation on Vertical Array	σ_{α_y} = 95	μrad
Average of Magnitude	$\lvert\overline{d}\rvert$ = 87	μrad
Standard Deviation of Magnitude	$\sigma_{\lvert\alpha\rvert}$ = 110	μrad
Correlation of Magnitude and Power	r_α = -31%	
Spot Diameter		
Diffraction Limit	W_D = 240	μrad
Mean on Horizontal Array	$\overline{W_x}$ = 230	μrad
Mean on Vertical Array	$\overline{W_y}$ = 230	μrad
Standard Deviation on Horizontal Array	σ_{W_x} = 23	μrad
Standard Deviation on Vertical Array	σ_{W_y} = 25	μrad

RUN 36

Aperture Diameter	$D = 7$ mm
Path Length	$L = 100$ m
Turbulence Strength	$C_n^2 = 3.5 \times 10^{-13}$
Inner Scale	$l_o = 6.6$ mm
Fresnel Zone Size	$\sqrt{\lambda L} = 9.1$ mm
Phase Coherence Length	$\rho_o = 1.5$ cm
Scintillation Index	$\beta = 0.087$
Signal Power	
Calculated Variance	$\sigma_s^2 = 0.073$
Measured Variance on Horizontal Array	$\sigma_{s_x}^2 = 0.044$
Measured Variance on Vertical Array	$\sigma_{s_y}^2 = 0.044$
Angle-of-Arrival	
Calibrated Single-Axis Standard Deviation	$\sigma_\alpha = 14$ μrad
Measured Standard Deviation on Horizontal Array	$\sigma_{\alpha_x} = 18$ μrad
Measured Standard Deviation on Vertical Array	$\sigma_{\alpha_y} = 21$ μrad
Averaged Magnitude	$\lvert\bar{d}\rvert = 23$ μrad
Standard Deviation of Magnitude	$\sigma_{\lvert\alpha\rvert} = 13$ μrad
Correlation of Magnitude and Power	$r_\alpha = -1\%$
Spot Diameter	
Diffraction Limit	$W_D = 100$ μrad
Mean on Horizontal Array	$\bar{W}_x = 170$ μrad
Mean on Vertical Array	$\bar{W}_y = 190$ μrad
Standard Deviation on Horizontal Array	$\sigma_{W_x} = 8.9$ μrad
Standard Deviation on Vertical Array	$\sigma_{W_y} = 11.6$ μrad

RUN 37

Aperture Diameter	$D = 3$ mm
Path Length	$L = 100$ m
Turbulence Strength	$C_n^2 = 2.6 \times 10^{-13}$ $m^{-2/3}$
Inner Scale	$l_o = 7.2$ mm
Fresnel Zone Size	$\sqrt{\lambda L} = 9.1$ mm
Phase Coherence Length	$\rho_o = 1.8$ cm
Scintillation Index	$\beta = 0.066$
Signal Power	
Calculated Variance	$\sigma_s^2 = 0.064$
Measured Variance on Horizontal Array	$\sigma_{s_x}^2 = 0.044$
Measured Variance on Vertical Array	$\sigma_{s_y}^2 = 0.048$
Angle-of-Arrival	
Calibrated Single-Axis Standard Deviation	$\sigma_\alpha = 14$ μrad
Measured Standard Deviation on Horizontal Array	$\sigma_{\alpha_x} = 24$ μrad
Measured Standard Deviation on Vertical Array	$\sigma_{\alpha_y} = 23$ μrad
Average of Magnitude	$\lvert\overline{d}\rvert = 29$ μrad
Standard Deviation of Magnitude	$\sigma_{\lvert\alpha\rvert} = 16$ μrad
Correlation of Magnitude and Power	$r_\alpha = 16\%$
Spot Diameter	
Diffraction Limit	$W_D = 240$ μrad
Mean on Horizontal Array	$\overline{w}_x = 220$ μrad
Mean on Vertical Array	$\overline{w}_y = 240$ μrad
Standard Deviation on Horizontal Array	$\sigma_{w_x} = 7.8$ μrad
Standard Deviation on Vertical Array	$\sigma_{w_y} = 12.5$ μrad

RUN 38

Aperture Diameter	D	= 7	mm
Path Length	L	= 9	km
Turbulence Strength	C_n^2	=	
Inner Scale	l_o	=	
Fresnel Zone Size	$\sqrt{\lambda L}$	= 8.6	cm
Phase Coherence Length	ρ_o	=	
Scintillation Index	β	=	
Signal Power			
Calculated Variance	σ_s^2	=	
Measured Variance on Horizontal Array	$\sigma_{s_x}^2$	= 2.2	
Measured Variance on Vertical Array	$\sigma_{s_y}^2$	= 2.3	
Angle-of-Arrival			
Calibrated Single-Axis Standard Deviation	σ_α	=	
Measured Standard Deviation on Horizontal Array	σ_{α_x}	= 370	μrad
Measured Standard Deviation on Vertical Array	σ_{α_y}	= 290	μrad
Average of Magnitude	$\lvert\overline{d}\rvert$	= 310	μrad
Standard Deviation of Magnitude	$\sigma_{\lvert\alpha\rvert}$	= 360	μrad
Correlation of Magnitude and Power	r_α	= -31%	
Spot Diameter			
Diffraction Limit	W_D	= 100	μrad
Mean on Horizontal Array	$\overline{w}_x$	= 190	μrad
Mean on Vertical Array	$\overline{w}_y$	= 190	μrad
Standard Deviation on Horizontal Array	σ_{w_x}	= 24	μrad
Standard Deviation on Vertical Array	σ_{w_y}	= 24	μrad